NTNU
Norwegian University of
Science and Technology

Implementation of Permanent Magnet Motors in Electric Vehicles

Eirik Elvestad

Master of Science in Energy and Environment
Submission date: June 2008
Supervisor: Tom F. Nestli, ELKRAFT

Problem Description

The use of Permanent Magnet machines in electric vehicles is interesting due to the machine type's compactness and low weight. However, contrary to the case with induction and reluctance machines, the permanent excitation is a concern in fault situations and has to be handled with care.

The thesis will adress implementation of PM motors in electric vehicles, with focus on design requirements, controls and how to handle faults in a feasible way.

Assignment given: 22. January 2008
Supervisor: Tom F. Nestli, ELKRAFT

Abstract

This thesis has studied permanent magnet motors in electric vehicles (EVs) under the assumption that they are tractable due to a low weight and high compactness. The implementation has been investigated through a case study, which resulted in an EV simulation model. The model contains a maximal torque per ampere and a closed-loop field weakening controller.

Faults are a special concern in permanent magnet motors. Fault sources and faulted behavior are addressed separately. The EV model was used to simulate faulted behavior.

Two passive fault measures are suggested as the most attractive for propulsion purpose motors; these are shutting down the inverter and imposing a balanced short to the machine terminals. The balanced three phase short circuit showed a considerable transient behavior not seen during inverter shutdown. This results in an increased requirement to the inverter rating using the balanced short. Also, demagnetization risk of rotor magnets is higher under the balanced short.

The maximal braking torque during inverter shutdown was high for the simulation model, and exceeded the braking torque of any fault. This concern led to a mathematical examination of the inverter shutdown, resulting in two equations that may be of use during design. The resulting equations are based on simplifications done in the literature, and show the relationship of the balanced short to the inverter shutdown.

Preface

This thesis is the result of five years of studying energy and environmental engineering, with specialization electric power engineering. During the last year, I have written one project and this thesis for the Energy Conversion Group (ENO) at the Department of Electric Power Engineering here at the Norwegian University of Science and Technology (NTNU).

After five years at NTNU and TU Dresden, I am grateful to the lectures who have made me first of all curious. I think I see the power of the tools that I have learned, and I am anxious to see if I can get them to work in real life. I realize that as a master student, I really know much less than I though I knew coming out of high school.

I would like to thank my supervisor, Tom Nestli, for his practical and down-to-earth comments, which inspired me to try to combine industrial feasibility with what I have learned and the articles that I have read.

Eirik Elvestad
July 17 2008
Trondheim, Norway

List of Abbreviations, Symbols, Sub- and Superscripts

Abbreviations

EMF   electromotive force

EV   electric vehicle

IC   internal combustion

IPM   interior permanent magnet (machine)

PM   permanent magnet

PWM   pulse width modulation

SPM   surface permanent magnet (machine)

UCG   uncontrolled generator (behaviour)

VA   volt-ampere (rating)

VSI   voltage source inverter

Sub- and superscripts

3ph   three phase

a   active damping (used toghether with axis subscripts q and d)

ag   air gap

base base quantity

d   direct axis

i   integral term

p   proportional term

q   quadrature axis

ref   reference

s	stator
sat	saturation
sc	short circuit
wh	wheel

Symbols

B	flux density
E	electromotive force
F	force
γ	field weakening controller gain
I, i	current
J	intertia
L	inductance
l	length
λ_m	peak magnet flux linkage (assumed sinusoidal)
m	mass
n_p	number of pole pairs
ω_r	rotational speed of the rotor, motor viewpoint, electrical degrees
P	power
r	radius
R	resistance, reliability
s	laplace variable
T	torque
v	voltage, speed
ξ	rotor saliency ratio L_d/L_q

x

Contents

Chapter 1

Introduction

In this chapter, the context of permanent magnet motors in electric vehicles will be briefly introduced. This will include an historical viewpoint, and a brief summary of work previously carried out. In addition, the motivation and goal for the current investigation will be stated.

1.1 The electric vehicle

The idea of an electric vehicle (EV) is not a new one. Already in 1830, the first vehicles were demonstrated, and they were about as popular as petrol cars with internal combustion (IC) engines up to about 1910, when the oil prizes fell. Today's popularity of petrol can be understood realizing that petrol may store up to 300 times more energy per weight than a battery. Taking the reduced efficiency of the IC engine into account, petrol will still provide driving ranges that exceed those of the electric vehicle.

With growing environmental concerns and improvements in battery technology, electric vehicles may gain new popularity. Pure electric vehicles have zero tailpipe emissions, and are energy flexible since they are fed from the electric grid. Both batteries and hydrogen solutions are predicted as energy carriers for electric vehicles in the future. These solutions both require an electric motor to transform electric energy to mechanical energy.

1.2 Why permanent magnet machines?

One of the really substantial differences between traditional (induction) electric motors and internal combustion engines may be found looking at the torque to weight and volume ratios, and the average to peak power capability. In both these senses, the internal combustion engine outperforms the induction motor [42].

The permanent magnet (PM) machine has got a low weight and can be made significantly smaller and lighter than induction machines for the same torque and power. The peak to average power is generally better than induction machines, but depends on the design.

The main reason why permanent magnet machines are more compact than for example induction and reluctance machines, is that excitation by permanent magnets is more compact than using current. In addition, current excitation needs cooling, which further increases mass and volume.

1.3   Previous work

Permanent magnet motor implementation in electric vehicles has been studied in the literature. In 1997, an axial flux PM machine was used in a concept solar race car, and demonstrated the potential efficiency of PM technology [41]. In the same article, means of increasing the base speed was suggested, and has been addressed in [27] and [25]. Faulted behavior of vehicle traction drives was addressed in [21], where the balanced short was suggested as a fault mitigation method. As almost a cookbook to control implementation of PM motors in automotive applications, [28] will be a much used reference in this thesis. It also addresses the faulted behavior of PM motors, together with some fault tolerant topologies. In [40] and [39], it was argued that the PM machine, with some design restrictions, can be made with the same fault tolerance as switched reluctance drives, though more compact. In addition to these articles, many others adress PM machines directly, or other aspects of electric power engineering in electric vehicles. Some of them will be used in this thesis, and are given in the reference list.

As an introduction to this masters thesis, an introductory project has been written [5]. The project argues that PM machines will be a compact and tractable choice in electric vehicles. It also introduces some design concepts of permanent magnet machines, some of them will be repeated in this thesis. The claim that PM motors are tractable in electric vehicles, will therefore be treated as a presumption in this thesis.

1.4   The goal of this thesis

The goal of the present thesis is to investigate the realization of permanent magnet machines for propulsion purpose in electric vehicles. An introduction to the drive demands and design regimes shall be made. It is a goal to make a typical model of an electric vehicle, that can be used for implementation discussion and fault analysis.

Faults shall be considered specifically, in order to point out concerns that have to be addressed during design stages. Passenger safety is the ultimate concern in fault situations. Practical fault measures shall be discussed and presented.

The current thesis is a presentation of publications on permanent magnet machines and their control, with focus on their use in electric vehicles and on faults. Simulation results are presented and used to strengthen the discussion on faults and their mitigation measures.

Faults were shortly addressed in the introductory project, and two mitigation methods were mentioned. The balanced short and inverter shutdown followed by

adjustable DC link voltage will be further investigated.

1.5   Outline of thesis

Chapter 2 will present introductory theory to the implementation of PM machines in electric vehicles. The vehicle model is presented along with the theory.

Chapter 3 presents theory and simulation results on faults. This will include classification, identification of the main sources to faults, and faulted behavior.

Chapter 4 presents fault mitigation methods from the literature, along with an introduction to fault detection.

Chapter 5 discusses fault handling in permanent magnet motors for traction applications. Some design trade-offs and suggestions will be presented.

Chapter 6 contains the key findings of this thesis.

Chapter 2

Design and operation

Vehicle propulsion has special demands on the drive. This chapter shortly introduces these demands, together with their design and operation specific consequences. Design regimes are briefly presented together with control basics, and used to introduce the electric vehicle model which will be used throughout this thesis.

2.1 PM machine fundamentals

In permanent magnet machines, torque is generated by two mechanisms. Force generated by the interaction of current and magnetic flux, called the magnetic torque, may be calculated by

$$F = B_{ag}Il \tag{2.1}$$

The uniqueness of the permanent magnet machine, is the free source of air gap flux B_{ag} created by the permanent magnets. The other source of torque, called the reluctance torque, comes as a result of a preferred magnetic direction in the rotor, called saliency. A preferred magnetic direction may be designed using that permanent magnets have high magnetic resistance (reluctance).

By Faraday's law, varying magnetic fields induce voltage, and for a conductor moving in an electric field, this induced electromotive force is,

$$E = B_{ag}lv \tag{2.2}$$

2.2 Desired torque-speed characteristics

The in-printed experience driving cars equipped with conventional engines, is the requirement of a high torque at low speeds for accelerating, and a lower torque at higher speeds for cruising [37]. Because internal combustion engines themselves have quite narrow torque-speed characteristics, a variable reduction gear is used to complete the torque-speed characteristic for all speeds. Using a gear, about the

same amount of power, depending on losses in the gear, can be delivered at a higher torque and lower speed, or vice versa.
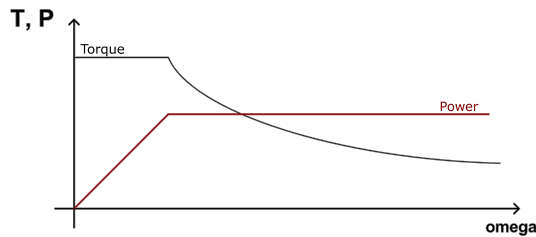
Figure 2.1: Desired power- and torque-speed characteristic for vehicle motors.

Electric motors typically exhibit the desired characteristic inherently. In the base speed region, a high torque can be demanded, limited by the current rating, which is mostly a thermal constraint. In this region, the supplied voltage increases linearly with speed. Above base speed, no more voltage can be utilized. Working at the voltage limit, speed can be increased by field weakening[1], where a higher speed is achieved on the cost of a lower torque.

Since the size of an electric motor is mostly torque dependent, using a gear can reduce motor mass and volume significantly. Because torque can be delivered at zero motor speed, this gear can be fixed.

2.3 High speed operation - field weakening

As commented, delivering power at high speed can significantly reduce the required motor size and weight, since motor size is mostly torque dependent. Because of this, and the reduced requirement of torque at high speed, operation in field weakening is very relevant for operation in electric vehicles.

Field weakening is achieved when the phase currents lead the induced EMF. In this situation, armature reaction in the machine acts to oppose the flux linkage produced by the magnets [1]. Armature effect (or reaction) can be described as the stator current's ability to interferer with the air gap flux. Therefore, in order to have good field weakening capability, the armature reaction effect needs to be large.

---

[1]A more correct term would be "flux weakening", since it is the air gap flux that is being weakened. However, field weakening seems to be the usual term in the literature, and will be used in this thesis.

(a) $i_d = 0$
machine optimal

(b) $i_d < 0$
flux weakening
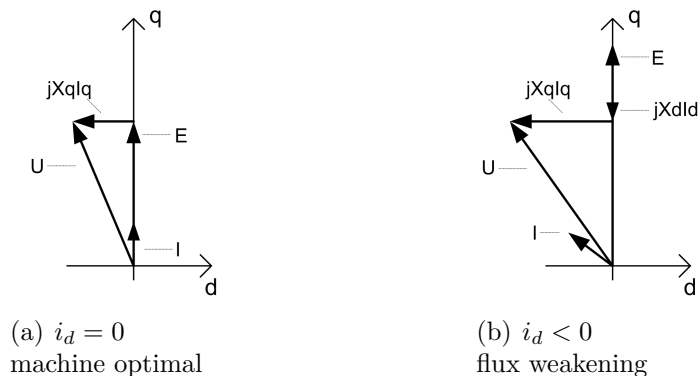
Figure 2.2: Phasor diagram illustrating field weakening in a non-salient machine. T_e constant; ω_r higher in (b); stationary conditions

Since field weakening in permanent magnet machines is done driving field current into the machine, current transportation losses increase. The field current may be utilized to create torque, if the machine is designed with negative saliency. Because of this, in [43], highly salient machines were argued to have the best field weakening possibilities.

The need to work in field weakening operation may be reduced by adding a variable gear to the drive train, a solution chosen in the Tesla roadster electric vehicle [Tesla Motors(2008)].

2.3.1 Increasing the base speed region using voltage

The base speed region can be extended by increasing the maximum phase voltage, as suggested in [41] and [25]. This can be done by adding a boost converter to the DC link. A conventional hard switched boost converter submits energy from a current source to a voltage source. That is, the boost converter "pumps" current from a lower to a higher electric potential. The ability to force current to a higher electrical potential requires an inductance to be fitted to the DC link, increasing the cost, weight and part count of the drive train.

Actively Clamped Resonant DC Link Converter with Boost.

Figure 2.3: The actively clamped resonant DC link boost converter from [27], used to extend the base speed. A hard switched boost converter uses the same principle, but would not require the upper part of the circuit (gray box).

In [27], a resonant DC link with boost capability is realized using an LC-resonance circuit and controlled switches. Resonant boost converters use the same

basic idea as the traditional hard switched converter, but switching losses are minimized due to the soft switching.

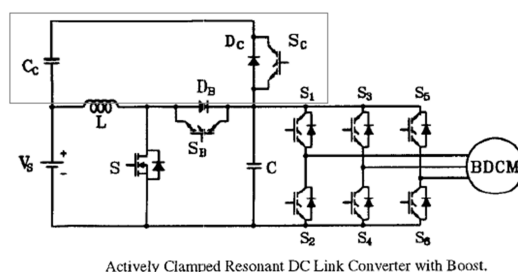The DC link voltage may be utilized better if it can be used over the entire phase. Using individual H-bridges for each phase will increase the maximum available voltage by a factor of $\sqrt{3} \approx 1.73$. A volt-ampere silicon-cost ratio was introduced in [33], and used to show that a dual-inverter solution has a cost factor of 115% over the traditional 3-phase inverter, assuming that the prize is directly proportional to the VA-rating of power electronics.

2.4 Machine design

Permanent magnet machines may be divided into two main types from the shape of the back EMF. Machines with trapezoidal-shaped back emfs, driven by trapezoidal shaped line currents are called brushless DC (BLDC) machines. Synchronous permanent magnet machines (PMSM) are driven with sinusoidal line currents, and have sinusoidally shaped back emfs. Synchronous machines are claimed to have less torque pulsation than BLDC machines [14], especially during field weakening operation. The focus in this thesis will be on the synchronous machine. However, the same basic principles exist for both type of machines.

Different design regimes exist for permanent magnet machines. Typically, a division into interior permanent magnet (IPM) and surface permanent magnet (SPM) motors can be made.

2.4.1 Surface mounted PM machines
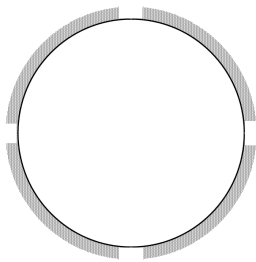
Figure 2.4: Surface mounted permanent magnet rotor.

Surface permanent magnet machines have large effective air gaps, and therefore require strong (high coercive force) magnets. Because of the large effective air gap, armature reaction effects are usually small. Due to small armature effects, these machines have traditionally been considered poor candidates for field weakening operation [27]. However, new design methods exist for SPM machines with high speed capability [38]. These machines use concentrated windings and the fact that, for the same flux linkage, armature inductance (effect) can be made significantly higher with concentrated windings.

SPM machines have simple designs, and may be constructed with high pole numbers to minimize iron and copper weight and volume. In a comparison carried out in [38], the SPM machine is significantly smaller than the interior PM machine.

2.4.2 Interior mounted PM machine

Interior permanent magnet machines are made with smaller air gaps and have larger armature effects. They have traditionally been considered the natural choice for high speed applications [43]. IPM machines can be equipped with lower performing magnets, using flux concentration and a small air gap with lower reluctance. A reluctance torque component can be utilized if negative saliency is constructed using the permanent magnets. Methods exist and are being explored to increase the saliency ratio and thereby utilize more reluctance torque [13], which is especially tractable in the field weakening region.
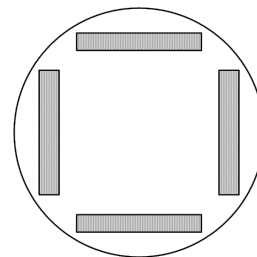
Figure 2.5: Interior mounted permanent magnet rotor.

2.4.2.1 Radially mounted interior PM machines

A special case of the IPM machine is the radially mounted machine. This machine has positive saliency, i.e. it has a higher reluctance in the q-axis than in the d-axis. Therefore, these machines behave more similar to traditional wound-field motors than to PM machines with negative saliency. Since the reviewed literature and the simulations are carried out for machines with negative saliency, the results will have limited accuracy for this type of machine.
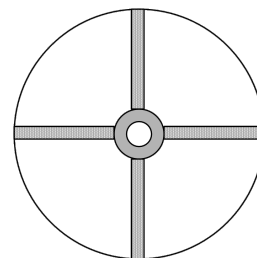
Figure 2.6: Radially interior mounted permanent magnet rotor.

Based on this presentation, it is not generally possible to say what type of design an electric vehicle should have. SPM machines have the potential to be the most compact per torque, but IPM machines are still most common for high speed operation. In IPM machines, the magnets are protected from armature behavior [7], whereas in SPM machines with large armature effects, magnets may suffer from demagnetization under high currents due to overload or in a fault situation.

2.5 Controls

2.5.1 Machine description - controlled equations

When all harmonics in inductance variation and flux-linkage are left out (not simulated), the current dynamics are described by (see appendix, section B.2):

$$v_d = R_s i_d + L_d \frac{di_d}{dt} - \omega_r L_q i_q \tag{2.3}$$

$$v_q = R_s i_q + L_q \frac{di_q}{dt} + \omega_r L_d i_d + \omega_r \lambda_m \tag{2.4}$$

The d and q voltages are transformed to switching signals to the inverter using space vector modulation, (see section B.1 and [12]).

For a definition of of the dq axis system used in this thesis, see section A.2. The produced electromagnetic torque is derived from the co-energy:

$$T_e = \frac{3n_p}{2} \left[i_q \lambda_m + (L_d - L_q) i_d i_q \right] \tag{2.5}$$

2.5.2 Current control

The current controller is presented in [28, referring to a 3rd article]. The controller controls the d- and q-component currents (described by eq. 2.3 and 2.4). Since the motor is fed by a voltage source inverter (VSI) the controlled variables are the line voltages.

The control output are the d- and q-component voltages, and they are controlled as:

$$v_d^{ref} = \underbrace{k_{pd}(i_d^{ref} - i_d) + k_{id}\frac{1}{s}(i_d^{ref} - i_d)}_{PI-controller} - \underbrace{\omega_r L_q i_q - R_{ad} i_d}_{decoupling, \ damping} \tag{2.6}$$

$$v_q^{ref} = k_{pq}(i_q^{ref} - i_q) + k_{iq}\frac{1}{s}(i_q^{ref} - i_q) + \omega_r L_d i_d - R_{aq} i_q \tag{2.7}$$

With

$$k_{pd} = \alpha_c L_d, \quad R_{ad} = \alpha_c L_d - R_s, \quad k_{id} = \alpha_c^2 L_d$$

and

$$k_{pq} = \alpha_c L_q, \quad R_{aq} = \alpha_c L_q - R_s, \quad k_{iq} = \alpha_c^2 L_q$$

Choosing these parameters for the controller gains (as in [28]), the current axes are decoupled, and the resulting transfer functions are,

$$\frac{i_d}{i_d^{ref}}(s) = \frac{\alpha_c}{s + \alpha_c}, \qquad \frac{i_q}{i_q^{ref}}(s) = \frac{\alpha_c}{s + \alpha_c} - \frac{s}{L_q(s + \alpha_c)^2} \lambda_m \omega_r$$

See section B.4 for the derivation of the transfer functions. The bandwidth of the current dynamics are now chosen by α_c, and the disturbance from the back EMF is well damped.

2.5.3 Torque and speed control

For non-salient machines, full decomposition in field and torque for the current components is realized. Torque is only produced by adjusting the i_q current, and a torque reference may be directly translated to a q component current using equation 2.5:

$$i_q^{ref} = \frac{2T_e^{ref}}{3n_p\lambda_m} \tag{2.8}$$

Machines that have saliency can also produce reluctance torque, using both current components (eq. 2.5). For salient machines, it may therefore be favorable to have a controller outside the current controller that transforms a torque reference to both a d- and q-component current reference. A simple maximal torque per ampere controller will be presented for the EV model (section 2.6.2.1).

In this thesis it is assumed that the accelerator (gas pedal) is coupled to a torque reference. This can be defended by the experience driving conventional vehicles. Implementing a speed controller outside the torque controller (cascade) can be done if for example cruise control is adopted, or if the accelerator pedal is coupled to a speed reference. A speed controller is presented in [28].

2.5.4 Field weakening control

For high speed operation, field weakening is achieved by setting i_d negative. The amount of required field weakening current can be decided by an offline calculation and a feed forward controller (table, function etc.) from the speed. This method has the advantage that the i_d^{ref} will be quite calm, because of the mechanical inertia. However, deciding the i_d^{ref} current in advance also has some drawbacks; it is not robust to changes in parameters that may occur because of the operating conditions and other phenomena.

The second method requires an i_d current to limit the controller output voltage reference to stay below a maximal voltage of $V_{max} = V_{dc}/\sqrt{3}$, which is the maximum phase to neutral voltage the inverter can utilize (see section B.1).

A pure I-controller is used in order to avoid a direct algebraic loop, as proposed by [8];

$$\frac{di_d^{ref}}{dt} = \gamma \left(V_{max}^2 - (v_d^{ref})^2 - (v_q^{ref})^2 \right) \tag{2.9}$$

The controller output must be limited to $-I_{max} < i_d^{ref} < 0$, and the integrator clamped when these boundaries are met (anti wind up).

Delay of the field weakening controller and current controller will make the current controller request a voltage that exceeds the maximum output voltage, causing the inverter to over-modulate. When entering the over-modulation region, integral terms in the current controllers will wind up, typically causing current over-shoots. An anti wind up feedback to the integrators is suggested in [8].

Originally adopted for an induction motor [8], a suggestion for γ is presented. This value may be chosen as a starting point when tuning the controller.

2.6 Case study simulation model

During the work on this thesis, a car model was build in MATLAB/Simulink and PLECS. The simulation tools are shortly described in the appendix (section C.3). The EV model includes a machine and inverter, implemented in PLECS, a current controller and a field weakening controller. References to the simulation model is made throughout the text.

2.6.1 Motor and inverter

The car is equipped with an interior permanent magnet motor rated to 50 kW continuous power. A standard three-phase inverter with 6 switches is adopted, coupled to a battery and filter capacitor. The voltage at the DC link is 320 V. More data is presented in the appendix (sec. C.1). The motor is assumed to have no harmonics in the flux linkage or inductance distribution (ideal PMSM), and can be described using the equations presented in section 2.5.1.

The motor may be overloaded for shorter amounts of time, because of the thermal inertia. However, since the heat capacitance of power electronics is far below that of the motor, the inverter needs to be rated for continuous operation in overload. Due to this trade off between inverter rating and overload, an overload capability of 2 times the rated current is suggested for this motor. This will imply that the maximal torque is around 150 Nm, which is the same as for many ICEs that are fitted to smaller family cars, for example, the most common 1.6 liter petrol VW Golf [Volkswagen(2008)].

2.6.1.1 Inductance model

The simulated machine has no mutual inductance between the phases. This is not realistic for distributed winding arrangements. For a distributed sinusoidal winding distribution, and three fully pitched phase windings, the mutual inductance is $\frac{1}{2}$ of the self inductance[2]. For some combinations of slots per pole and phase, using concentrated winding arrangements, mutual inductance can be very low [38].

The simplification assuming no mutual inductance done for numerical reasons, since it reduces the amount of states when using PLECS, and significantly reduces the running time of the simulation. The implications of this assumption on the simulation will be addressed during the presentation of faulted behavior (section 3.4).

An inductance model for the EV model machine that accounts for the first harmonic of salient components is showed if figure 2.7.

---

[2]$L_m = \frac{1}{2}L_s$ since $\int_0^{2\pi} N(\theta) \cdot N(\theta + \frac{2\pi}{3})\,d\theta = \frac{1}{2}\int_0^{2\pi} N^2(\theta)\,d\theta$, for $N(\theta)$ sinusoidal. N is the winding distribution function.
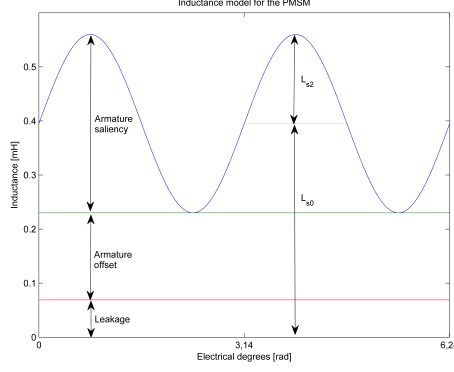
Figure 2.7: Illustration of the self inductance for an interior synchronous PM machine with only 2. order harmonics (saliency) included. This graph may be generated measuring the self inductance of one phase, while turning the rotor 2π electrical degrees.

A distinction between leakage inductance and inductance mutual to the rotor has been made. The rotor-mutual inductance interfere with the air gap flux and is called armature inductance. Rotor saliency is possible by changing the armature inductance of the axes in the rotor.

The d and q axis components of the inductance are derived from the periphery inductance by (see section B.2 and [28]).

$$L_d = L_{s,0} + \frac{L_{s,2}}{2} - L_{m,0} + L_{m,2} \qquad L_q = L_{s,0} - \frac{L_{s,2}}{2} - L_{m,0} - L_{m,2} \qquad (2.10)$$

Where the L-values are the amplitudes of the n-th harmonic of the self- and mutual inductance. Note that the $L_{s,2}$-term is negative for most types of salient PM machines, leading to $L_q > L_d$.

2.6.2 Adopted controls

The machine is equipped with the current controller presented in section 2.5.2, with $\alpha_c = 900$ rad/sec. The bandwith could have been increased further, but had to be relaxed to insure stability during saturation. The closed loop integral field weakening controller of section 2.5.4 was chosen with $\gamma = 0.5$.

Because the inverter current capability is limited, the input to the current controller is limited to $\sqrt{(i_d^{ref})^2 + (i_q^{ref})^2} \leq I_{max}$. The field weakening current i_d has the highest priority. The torque component i_q current is dynamically saturated. The saturation block is constituted so that

$$-I_{max} < i_d^{ref} < 0 \,, \qquad -\sqrt{I_{max}^2 - i_d^2} < i_q^{ref} < \sqrt{I_{max}^2 - i_d^2}$$

The current controller does not allow overload conditions, although the inverter was overrated for overload. Overload can be included in the current controller by adjusting I_{max}, for example using thermal sensors.

2.6.2.1 Simple max. torque per ampere strategy

The implemented motor has a saliency ratio $\xi = L_q/L_d$ of 2.43, so it is expected that the maximal achievable torque per ampere may be realized using both current components. To verify this, a simple non linear optimization problem was formulated in MATLAB, and solved using the optimization toolbox (see section B.5). Utilizing the full stationary current capability of the motor, the maximal torque was plotted against the speed (figure 2.8):
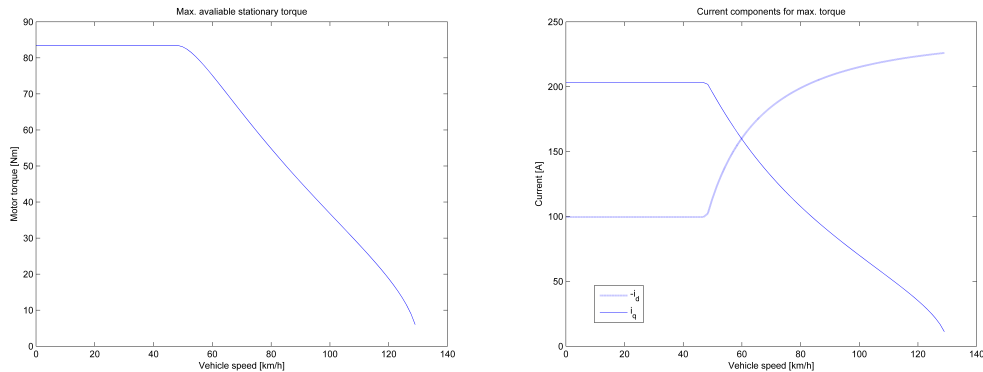
Figure 2.8: Maximal torque and corresponding currents. Note that the i_d current has been inverted in the plot.

This result may be compared to setting $i_q = I_{max}$, which would yield a maximal torque of 70.6 Nm. Further, the minimal current needed to produce 50 Nm of torque up to about 80 km/h was calculated. The result is depicted in figure 2.9. For
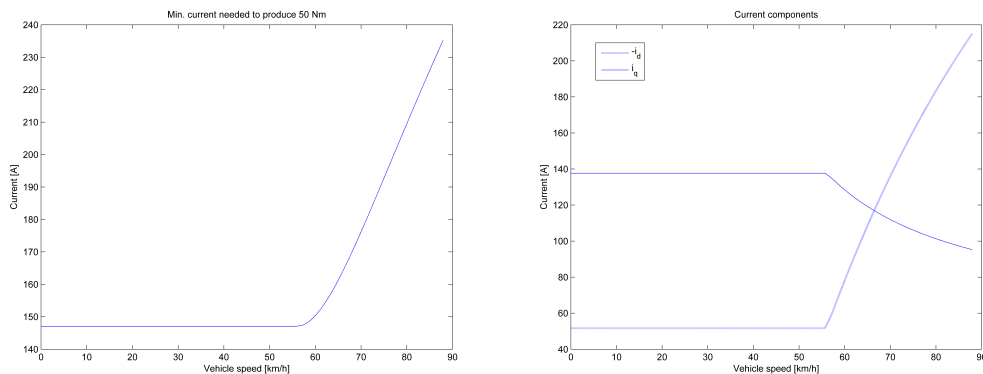
Figure 2.9: Minimum current needed to produce 50 Nm. Note that the i_d current has been inverted in the plot.

comparison, using only q component current would require $i_q = 160.2$ A to deliver the same amount of torque below base speed. Realizing that less current is needed to produce the same torque when both current components are activated, a simple controller was designed in order to minimize current transportation losses.

The optimization results reveal that the relationship between the optimal i_q and i_d current is a function of the torque below base speed. The optimization problem was therefore reformulated to identify the minimal current components as a function
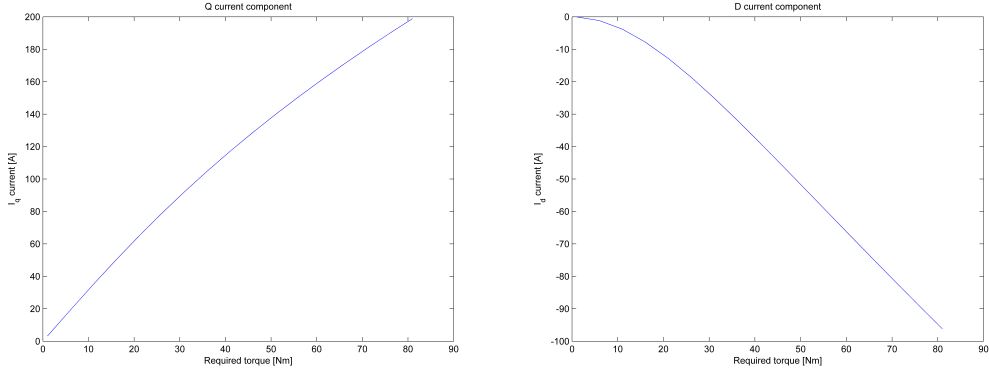
Figure 2.10: Minimum current needed to produce a required torque below base speed.

of the torque, at zero speed. Since the results of the optimization (figure 2.10) are relatively linear, a linear regression was carried out, and the current components where simply calculated by

$$i_d^{ref} = k_1 T_e^{ref} \qquad i_q^{ref} = k_2 T_e^{ref}$$

Where $k_1 = -1.28$, and $k_2 = 2.43$. This will not give a fully correct torque to current components reference, but since there are no controllers outside the torque controller, the approximation will not affect the stability.

Since i_d is also used for field weakening, the controller that requires the lowest i_d current decides the reference. This leads to a smooth transition into the high speed field weakening region, where the field weakening controller dictates the i_d current. This will imply that the k_2 gain should be altered for high speeds to give the correct torque reference, this is however not implemented in this model.

This maximum torque per ampere scheme is also straight forward to implement for overload capability. Carrying out the current optimization for up to 2 times rated torque results in the same nearly linear relationship between the currents. However, since i_d current may risk to demagnetize rotor magnets, and create very strong fields in the motor, it should be saturated at some value.

A long simulation was carried out with $T_e^{ref} = 80$ Nm. To speed it up, and prevent memory allocation failure, a relatively noisy solver had to be chosen, so the results needed to be filtered. They are shown in figure 2.11. Torque is delivered near the current limit I_{max}. In field weakening, the maximum torque is somewhat below the optimal solution found earlier, but only differs with 5-10 Nm.

2.6.3 Simulation circuit

The implemented circuit topology is depicted in figure 2.12.

The PMSM model that is implemented in PLECS consists of three inductances and resistors in series with back emfs.

In Simulink, the inverter and the PMSM machine where implemented in the PLECS block. The DC link was modeled as a Thevenin equivalent. The motor
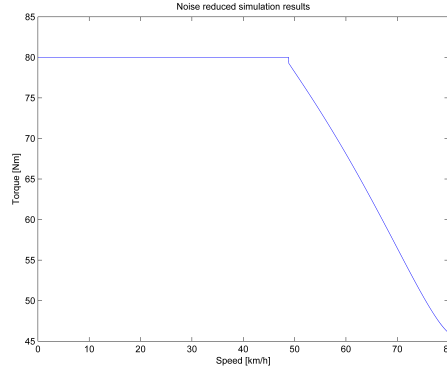
Figure 2.11: Simulation result to test max torque per ampere.
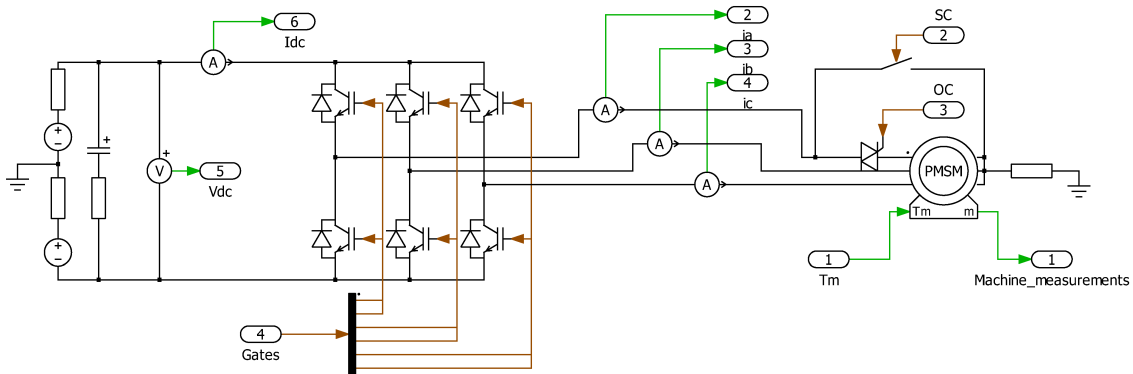
Figure 2.12: Connection setup of the PMSM used in the simulations

current and speed controller were implemented outside the PLECS circuit.

2.6.4 Mechanical parameters

The total vehicle mass is 1200 kg, and it has a fixed gear with a ratio 1 : 14 from the motor to the wheel.

The vehicle body and wheels is modeled as stiffly connected to the rotor shaft. The total equivalent shaft inertia is found by:

$$J_{tot} = J_m + \left(4J_{wh} + mr^2\right) \frac{1}{(\omega_r/\omega_{wh})^2} \tag{2.11}$$

For more data on the simulation model, see section C.2.

2.6.5 The difficulty of simulating unbalanced conditions

Motor models of the PMSM found in simulation software are typically simplified to fit balanced operation. The simplifications typically do not account for;

- The non-zero neutral voltage, with respect to DC link center point. The neutral voltage does not coincide with the DC center voltage under unbalanced condition.
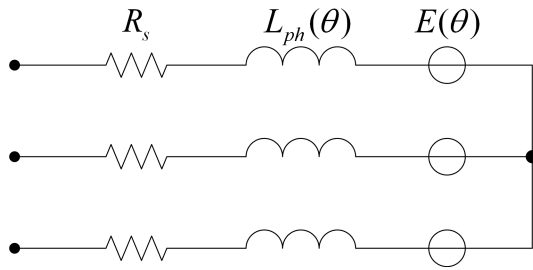
Figure 2.13: PMSM circuit used in simulations.

- The mutual inductance can easily be removed from the equations under balanced conditions. This is not the case in non symmetrical fault situations, where the behavior depend on the mutual inductance.

The behavior of a motor under unbalanced conditions is more design dependent that under balanced conditions. This implies that the simulation results will have limited accuracy for different PM machine designs.

Chapter 3

Faults

The concept of permanent excitation implies that electromotive force is permanently induced when the motor is in motion. Permanent excitation, though mostly desirable, has the ability to drive currents and create torques, and this is a concern if the motor suddenly comes out of control. This chapter will discuss the likelihood of faults, their classification and behavior. The results will join the discussion on fault mitigation.

3.1 Introduction

The excitation in a permanent magnet machine cannot be removed, and as a consequence, electromotive force will be induced as long as the rotor magnets are in motion. The permanent back EMF possesses the ability to drive currents, even when the controller and inverter are passive. In fault situations, permanent excitation may lead to uncontrollable and high torques and currents, that eventually influence passenger safety and could make faults escalate further.

In field weakening operation, the back EMF of the motor exceeds the terminal voltage, and if field weakening current is interrupted, the motor has the ability to force the voltage up on the DC link, and damage electrical components such as the inverter and the battery.

3.2 Fault classification

Faults occurring in the drive train can be classified into three categories: short circuit faults, open circuit faults and sensor faults. Fault mitigation techniques will be discussed based on the type of fault.

3.2.1 Open circuit faults

Open circuit faults may occur in the inverter and in the motor. In addition to the two single phase faults, inverter shutdown also falls into this category.

Single-switch open circuit is the situation in which the transistor fails to be turned on, but the integral diode is still intact.

(a) Single switch open circuit   (b) Full phase open circuit   (c) Inverter shutdown
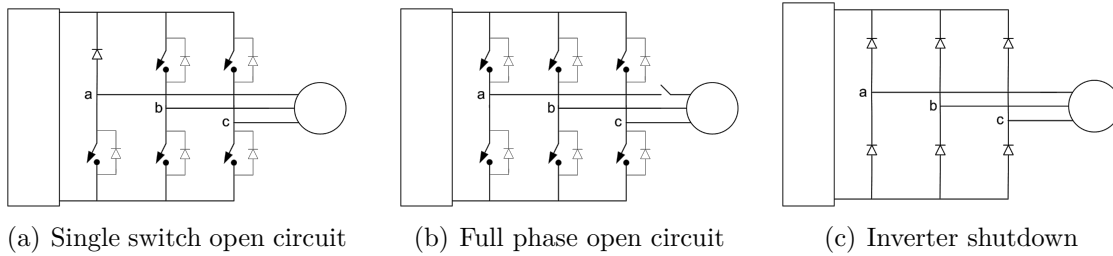
Figure 3.1: The different open circuit faults

True open circuit is different from the single-switch case because the free-wheeling diode is no longer present, and the motor phase is fully disconnected from the inverter.

Inverter shutdown is the equivalent situation of a motor directly connected to an uncontrolled diode rectifier.

3.2.2 Short circuit faults

Short circuit faults may also occur in the inverter and motor. The three phase balanced short circuit is also included in this category. Short circuit faults in the winding arrangement of the machine include short circuits between windings of the same phase, winding and the chassis, and between windings of different phases.

Single-switch short circuit is created when one of the inverter transistors are permanently gated on.

Phase-to-phase short circuit may occur at different places in the affected phase windings, and is hence a family of faults in it own.

Intra-winding shorts occur between turns of the same winding.

Phase-neutral short circuit is the situation in which the phase terminal is directly connected to the neutral point of the motor. It may be considered as a special extreme case of the intra-winding short circuit, where all the turns have been shorted.

Balanced three phase short circuit may be imposed by gating either all upper (ppp) or lower (nnn) transistors in the inverter.

3.2.3 Sensor faults

Sensor faults are presented in [15]. The motor must be equipped with current sensors on at least two of the phases. In addition, a DC link voltage sensor and an angle sensor may be adopted to the drive to increase the system stability. A fault in any of this sensors will affect the decision made by the control unit, finally influencing the physical behavior.

3.2.4 Mechanical faults and rotor faults

Faults in the rotor, due to for instance a bent shaft or corrosion of permanent magnets can influence the air gap flux. Such type of faults will not be treated in this thesis, as only electrical faults are investigated.

3.3 Fault sources

What can cause a fault situation in the drive train, and how likely are the various fault situations to occur? Although passenger safety must be insured for any type of fault, different faults must be considered together with their expected occurrence frequency. It is expected that fault mitigation techniques may not be economically motivating if the likelihood of the fault is minimal and passenger safety is insured.

It is evident that the electric vehicle is a harsh environment. Mechanical influence by the surroundings include considerable vibrations, dust, humidity and difference in ambient temperature. Without statistics and information regarding the specific designs, only a conceptual discussion on faults and their occurrence can be carried out.

3.3.1 Inverter faults and lifetime

Determining the lifetime of the inverter in an electric vehicle is difficult. Difference in thermal expansion of bond wire metal and silicon results in mechanical stress under thermal cycling, causing the bond wire to eventually loose contact with the chip. This effect is frequent for appliances where the inverter experience much thermal cycling, which is common in EVs because of the variety in load conditions. Individual differences also exist because each vehicle is driven differently. This type of fault is expected to be a dominant mechanism in the inverter in an electric vehicle [28, 4]. The common fault following from the bond wires loosing contact with the chip, is the full phase or switch open circuit.

In [11], a simulation model is made to observe thermal cycling and operating temperature of IGBTs used in hybrid electric vehicles. This model uses an advanced loss model and thermal cycle detecting algorithm, together with a driving cycle standard (suburban driving cycle). The area of reliability of power electronics in automotive applications seems to be active on the research agenda [28].

A failure of the gating unit to gate the transistors, will create a switch open circuit. The reliability of the gating unit will not be commented here, but must be considered in the combined reliability of the inverter.

A short circuit fault in the inverter can also follow from a fault in the gating unit. IGBTs contain a parasitic thyristor that can be turned on under high amounts of current (typically short circuit). If turned on, this thyristor cannot commanded off. However, the likelihood of such "latching" in modern IGBTs is small.

The load changing test ("Lastwechseltest" [20]) is used to determine the amount of thermal cycles a component can withstand before it fails. The cumulative prob-

ability for the amount of cycles before a component fails, is well described by the Weibull function [20]. It is well-known in the field of redundant systems, that an increased part count generally reduces the total reliability of the system [11]. To illustrate this for the inverter, defining the reliability function $R_j(t)$ to be the probability that a switch still functions after the time t, the total system reliability is defined by

$$R_{tot}(t) = \prod_{i=1}^{n} R_j(t) \tag{3.1}$$

If the main failure mechanism of the inverter is due to thermal cycling, the reliability of the inverter may be well modeled by the Weibull distribution. Using data from [20], the reliability can be approximated and compared for the amount of switches n:
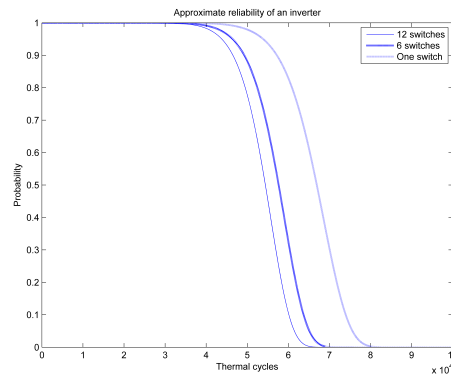
Figure 3.2: The probability that the component or inverter has not failed due to thermal cycling after a number of thermal cycles. Data for one switch from [20].

In addition, all other fall out-mechanisms that are not accounted for here, will reduce the total reliability and increase the difference due to the part count. It is clear that, under the assumption that the reliability function of the switches are equal, a larger part count will reduce the total system reliability. This will probably have the effect that the inverter must be replaced earlier, which has further implications for the manufacturer.

3.3.2 Machine failure

A considerable source of faults in the machine is expected to be short circuit faults in the armature. Short circuit faults in the armature (stator) are caused by insulation breakdown. Faults following from such breakdowns are usually phase-to-casing or phase-to-phase faults, that have been initiated by turn-to-turn short circuits [16, 10]. If much of the insulation in one phase is destroyed, and the turns shorted together, the phase will approach a short circuit to the neutral point of the machine. For induction motors, reliability test have shown that intra-winding shorts are a common reason for machine failure [22]. Many of the same failure mechanisms exist for permanent magnet machines:

Inverter fed machines experience voltage surges due to high frequency harmonics caused by rapid switching. Potential differences with steep flanks between turns stress the insulation. Phenomena such as partial discharge, dielectric heating and formation of space charges are known to occur [36]. These effects are design dependent, and can substantially influence the lifetime of the enameled wire in the machine. A typical result of electrical insulation stress is intra-winding short circuits in the first turns. Such an intra-winding short will produce heat which further evolves the short, so that phase-phase or phase-casing shorts can occur.

The though mechanical environment can initiate faults directly. Since the insulation of the enameled wire is thin, relative motion and friction between windings due to vibration may tear insulation leading to short circuit between turns.

In distributed winding arrangements, it is common that windings from different phases share the same slot. This significantly increases the likelihood of short circuits between phases.

Open circuit faults originating in the machine may be caused by mechanical failure of a terminal connector or an internal winding rupture [35].

3.4 Faulted behavior

The behavior of the drive under various types of faults is of particular interest in the implementation of a vehicle drive system. Together with various publications on faulted behavior of PM drives, the EV simulation model is used to model the behavior under faults. The goal is to identify faults that have to be mitigated, and maybe point at fault conditions that are less severe, or even temporarily tolerable.

The model used for simulations does not consider damping that occurs between the motor and vehicle. It is expected that this damping will affect the perceived vehicle behavior. To discuss the perceived operation driving the vehicle, the average torque will be calculated.

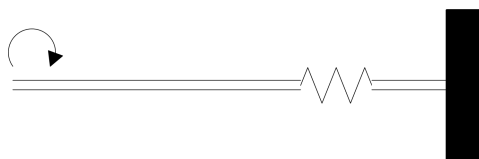Figure 3.3: Various rotational damping effects occur between gearing and wheel

In the simulation and following discussion, what interests the driver and manufacturer is related to safety and economy;

- What currents and torques occur in the given fault situation?

- Does the voltage increase on the DC link?

- Can the fault situation be sustained?

- Is the fault situation dangerous for the driver and passengers?

- Will the fault situation escalate and threat to destroy other components?

Stable fault conditions are preferable over oscillating ones. For the currents, even short over shoots can damage the inverter switches (to be commented in section 3.4.2). An oscillating torque can stress the mechanical parts of the vehicle, and be a threat to passenger safety.

The per unit quantities of current and torque can be found in the appendix (section A.1).

Mutual inductance. The simulation model does not contain mutual inductance between the phases. It is assumed that the general behavior of the faults that occur can be well simulated without the mutual inductance. For each phase, the back EMF will be present and contribute to a permanent current driving force when the motor rotates. When considering the ability for continued operation, the mutual inductance is important. The faulted phase can have circulating currents that affect the healthy phases if the mutual inductance is high.

3.4.1 Effect of q-axis saturation in IPM machines

Iron channels in the rotor q axis of interior permanent magnet machines (IPMs) may saturate under high levels of current, causing L_q to decrease. The saturation effect reduces the saliency of the machine, which acts to limit the torque and q component current under faults [13, 32]. To demonstrate what effect q axis saturation can have on simulation results, two simulations are compared under identical conditions. For machines that have low cross coupling effects between the q and d axis current, the saturating characteristic of L_q can be modeled as a function of the q axis current. Then, only the q axis voltage equation (eq. 2.4) needs to be altered;

$$v_{q-sat} = R_s i_q + \underbrace{(L_q(i_q) + \frac{\partial L_q}{\partial i_q} i_q)}_{\text{saturation term}} \frac{di_q}{dt} + \omega_r L_d i_d + \omega_r \lambda_m \qquad (3.2)$$

The new L_q-term in equation 3.2 accounts for the changes in magnetic stored energy. Mathematical models to fit the saturation characteristic can be found in [13] and [35]. The EV model IPM machine was fitted to a modified version of the model found in [35];

$$L_q = \begin{cases} C_1 |i_q|^{C_2} & \text{if } L_d \leq L_q \leq L_{q-max} \\ L_d & \text{if } L_q \leq L_d \\ L_{q-max} & \text{otherwise} \end{cases} \qquad (3.3)$$

For the derivative;

$$\frac{\partial L_q}{\partial t} = \begin{cases} C_1 C_2 |i_q|^{(C_2-1)} & \text{if } L_d \leq L_q \leq L_{q-max} \\ 0 & \text{otherwise} \end{cases} \qquad (3.4)$$

The C_1 and C_2 terms where adopted to fit the saturation data in [28] (see section C.1). Some minor modifications needed to be done to make the model stable. The middle term in eq. 3.3 was added to limit the amount of saturation to the d axis inductance. The d axis is chosen as a lower limit because it is limited by the relative permeability of the rotor magnets, which is equal to that of air. Because air does not suffer from saturation, it is expected that the inductance will stop saturating when the air value of the inductance is reached.

Results from a severe fault, a one switch short in the inverter, is compared in figure 3.4. The motor runs at 2000 rad/sec electrical, which is just above the base speed, while it delivers 35 kW. Here, the result shows that saturation acts to limit the peak torque by a factor of 7.5.
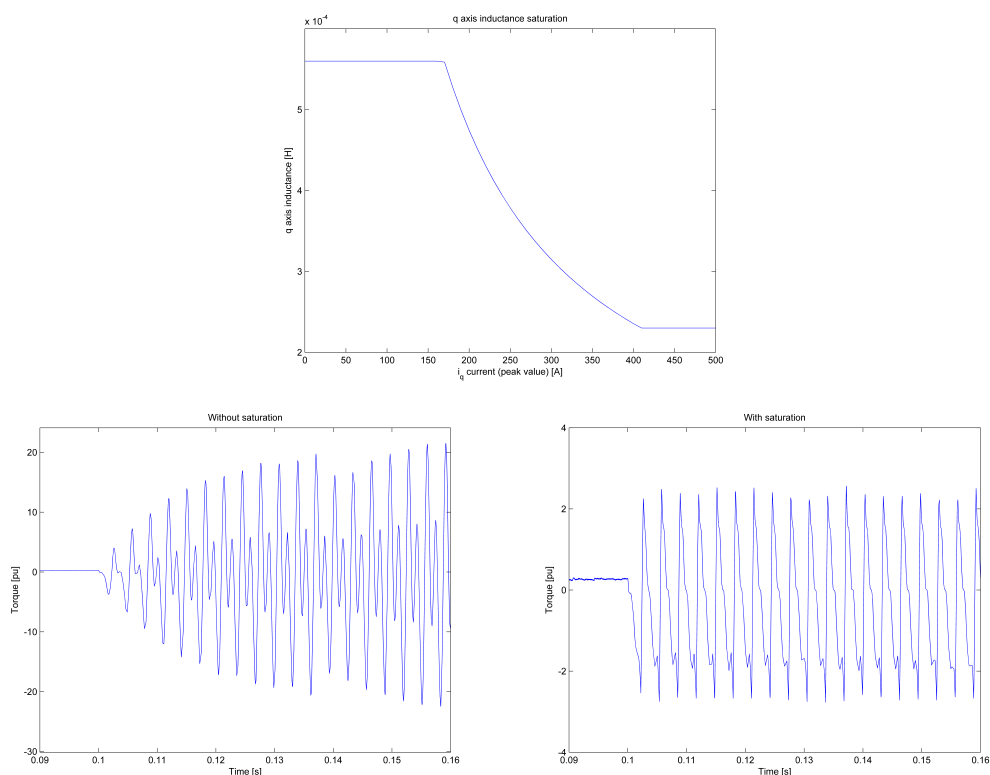
Figure 3.4: Simulation results showing the effect of q axis saturation

The result shows that the saturating characteristics of the q axis has a remarkable impact on the peak torque. It also strengthens the claim that the faulted behavior, because it is sensitive to saturation effects, depends on the design.

3.4.2   Saturation characteristic of a modern IGBT module

The EV model was chosen with an overload capability of twice the rated continuous current of the machine, to allow temporary overload operation. IGBTs have an absolute limit on their current carrying capability, the saturation current. It is not possible to carry a current above this level of current, so actually, IGBTs may be

good over current protectors. Note however, that thermally, power electronics can only sustain overload conditions for very short time periods.

Using a real life IGBT characteristic from the industry, as an install candidate for the EV model, typical data for modern IGBTs may be presented. IGBT modules typically start at 600 V blocking voltage. With a DC link voltage of 320 volts, this allows for considerable voltage peaks due to di/dt. The rated current for the module was chosen near the overload current, $I = 2\sqrt{2} \cdot 160 \approx 450$ A (2 pu).

Using data from eupec [Infineon(2008)], the "EconoDUAL™ Modul mit Trench/Feldstop IGBT3 und Emitter Controlled Diode 3" with $I_{DC} = 450$ A was chosen. Using a gate voltage of 15 V, this IGBT saturates around 2 kA, which it can withstand for 6 μs. It can resist repetitive peaks of up to 900 A (4 pu) for 1 ms .

3.4.3 The DC link stiffness and its role in fault situations

The DC link is modeled as a Thevenin equivalent for transient behavior, to estimate the voltage rise on the DC link during faults. The behavior of the DC link is mostly determined by the battery. If the voltage on the DC link rise too much during a fault, the battery and filter capacitor may be damaged, and the inverter voltage rating crossed. The simple Thevenin battery model that will be used for transient behavior was provided by Think [Think Global(2008)].

3.4.4 Single phase- and switch short circuit

This fault was examined in [32], where it was shown that saturation effects have a major influence on the faulted behavior. The results depicted in the article agree well with the results that have been simulated for the EV model.

Single switch short circuit. The inverter is shut down after the fault has occurred, to avoid a direct short of the DC link. The simulation has limited accuracy since the severity, with high currents and torques, makes rapid evolvement to open or other short circuits likely.
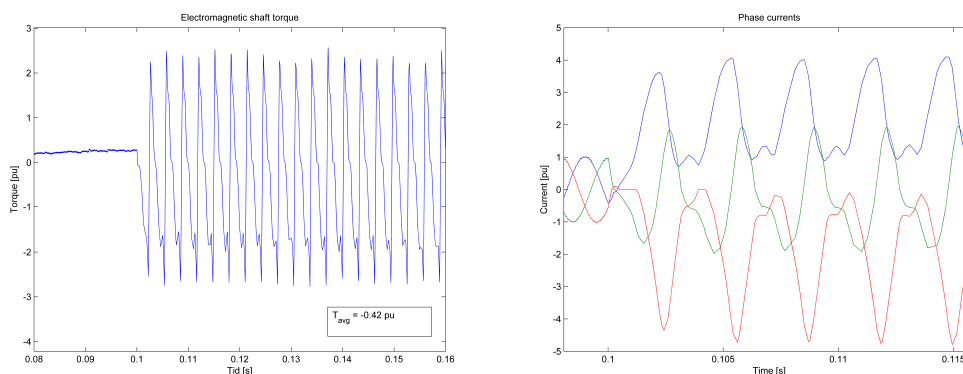
Figure 3.5: Simulation results of the single switch short circuit.

The faulted braking torque is around half the continuous torque, or 1/4 of the maximal torque. The high currents implies that the inverter and motor will be stressed, and it is not likely that this situation can be sustained for long. The intuitive consequence of inverter over current is the burn out of one or more transistors, resulting in an open circuit fault. Mechanical stress is high due to large torque amplitudes.

Phase terminal to neutral short. This is the extreme form of the intra-winding short circuit, and may result if a turn to turn short circuit is allowed to produce heat over time. After shutting down the inverter, the faulted torque is lower than for the
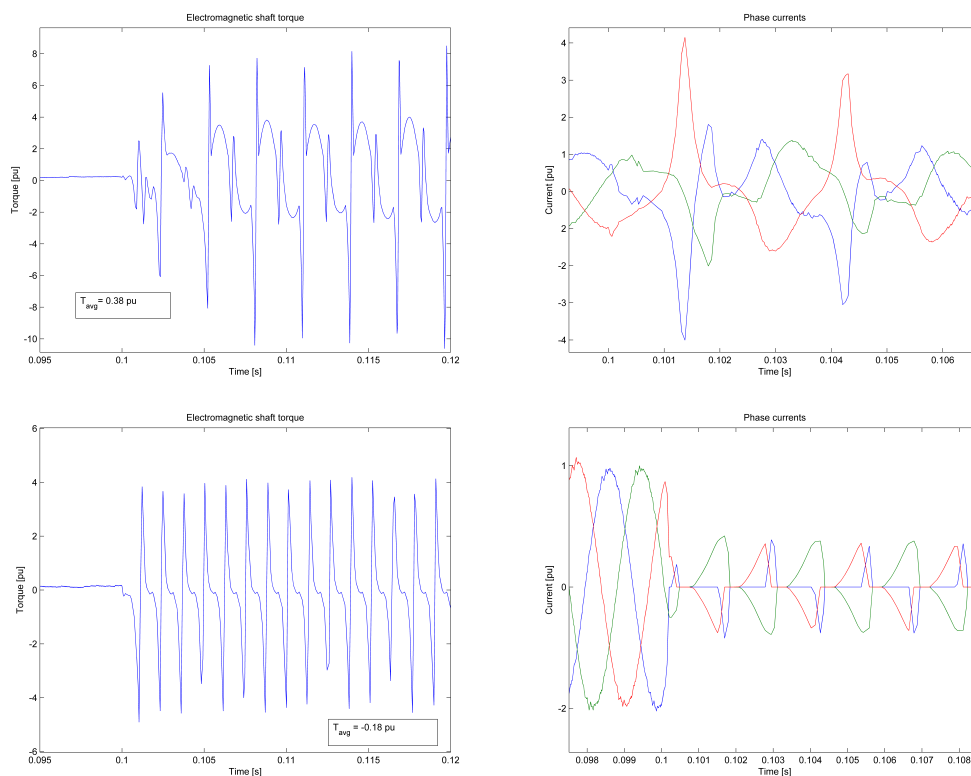
Figure 3.6: Simulation results of the single phase short circuit. With continued operation (top), and after inverter shutdown (bottom).

switch short circuit. Because of large torque amplitudes, mechanical stress will be high.

Phase-phase short circuit. The behavior of the phase-phase short circuit will depend on the location of the fault, and is difficult to simulate without a more detailed motor model. It is expected that this type of fault may span from a more severe behavior than the phase-to-neutral fault to a less severe one, depending on the parameters of the short circuited path. How-

Figure 3.7: Phase-phase short. Depending on the inductance and resistance of the short circuited path, and the flux linking it, a large circulating current can occur.

ever, since this fault includes more than one phase, it
may be a difficult fault to interrupt.

Intra-winding short circuit. If short circuits occur between neighboring turns,
it is not a severe fault in itself. Seen from the terminals of the motor, the inductance
only changes minimally, so the terminal currents and voltages will hardly change.
However, at the location of the short circuit, a large current will flow resulting in
high heat production.

3.4.5 Balanced three phase short circuit

Analytically derived stationary behavior. The balanced three phase short
is treated analytically in [32]. Stationary currents and torques can be found by
shortening the voltages in eq. 2.3 and 2.4. Setting time derivatives to zero yields
for the currents:

$$i_{d-3ph-sc} = -\frac{\omega_r^2 L_q \lambda_m}{\omega_r^2 L_d L_q + R_s^2} \tag{3.5}$$

$$i_{q-3ph-sc} = -\frac{R_s \omega_r \lambda_m}{\omega_r^2 L_d L_q + R_s^2} \tag{3.6}$$

$$\lim_{\omega_r \to \infty} i_{d-3ph-sc} = -\frac{\lambda_m}{L_d} \ , \qquad \lim_{\omega_r \to \infty} i_{q-3ph-sc} = 0$$

And for the torque:

$$T_{e-3ph-sc} = \frac{3n_p}{2} R_s \lambda_m^2 \left[\frac{-\omega_r}{\omega_r^2 L_d L_q + R_s^2} + (L_d - L_q)\frac{\omega_r^3 L_q}{(\omega_r^2 L_q L_d + R_s^2)^2} \right] \tag{3.7}$$

Because both the impedance and the back EMF increases linearly with speed,
the current asymptotes at high speed. Theoretically, seen from the equations, the
current will approach $-\lambda_m/L_d$ and be a pure d-component current as speed increases.
The total stator current increases monotonically with speed towards this asymptote,
as can be seen in figure 3.8;

It is claimed in [32] that the maximum braking torque occurs at $\omega_r = R_s/\sqrt{L_d L_q}$.
This seems to be an approximation. The actual expression is less pretty, and derived
in the appendix (section B.3). However, the expressions coincide for the non-salient
case, where

$$\omega_r = \frac{R_s}{L_s} \tag{3.8}$$

Calculating the maximum torque (using either eq. 3.8 or eq. B.10 in the ap-
pendix) reveals an interesting result. The maximum torque is independent of the
resistance (for both salient and non-salient machines). The resistance only influ-
ences the speed at which the maximum torque occurs. This is a result which will
have interest later. The maximum torque for the non-salient case is
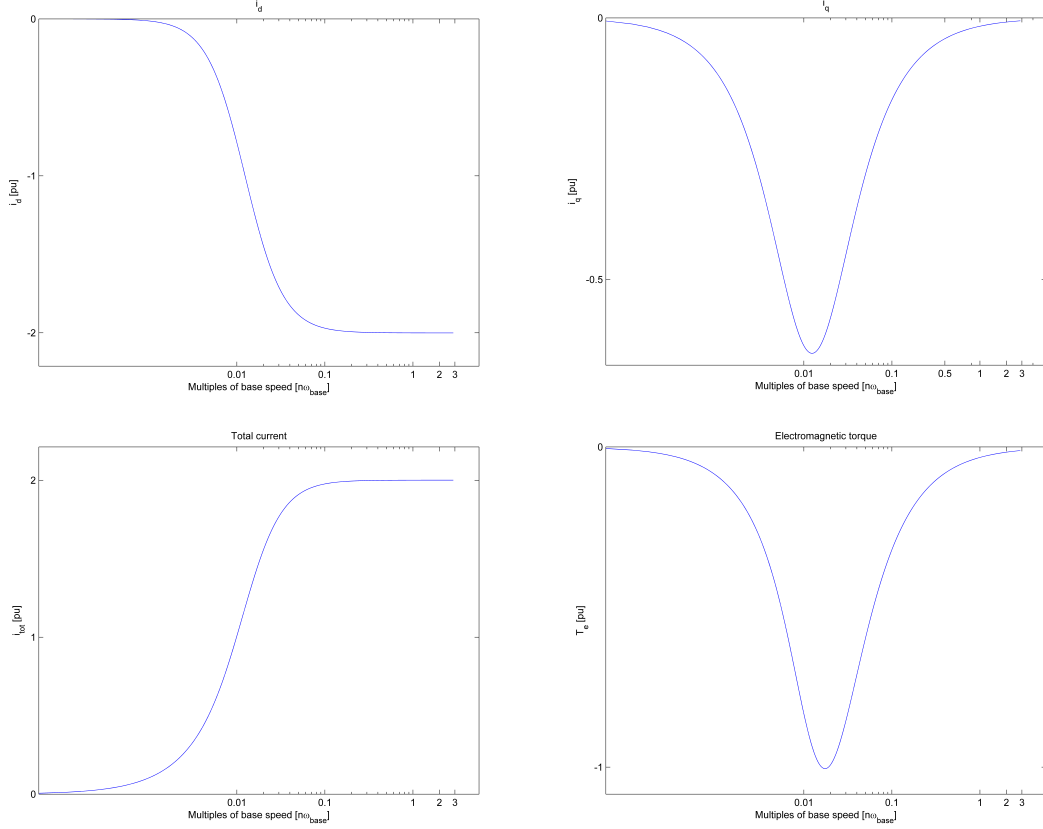
Figure 3.8: Results evaluating equations 3.5, 3.6 and 3.7 for the simulated machine. ω_{base} corresponds to 1776 rad/s electrical, and 65 km/h.

$$T_{max} = -\frac{3}{4}\frac{n_p\lambda_m{}^2}{L_s} \tag{3.9}$$

The expression is longer for salient machines, and is therefore given in the appendix (eq. B.11). It can be shown that the minimum braking torque occurs for the non-salient machine, under otherwise equal conditions.

Simulation model results. The maximum torque for the simulation model, calculated by eq. B.11 and B.10) is -83.4 Nm and it occurs at $\omega_r = 30.9$ rad/s, which corresponds to 1.3 km/h. Above this speed, the braking torque is rapidly reduced.

The theoretically derived expressions for the short circuit currents presented earlier do not account for the transient behavior. As seen in the simulation results of figure 3.9, transient peaks in current and torque is significantly higher than their stationary values.

The fluctuating torque during the transient is quickly stabilized and the amplitude is around the rated torque. This may result in vibrations and noise, but the mechanical behavior is not expected to be a source of concern to passengers.

In agreement with the results in [32], the transient d-axis current reaches values significantly higher than the characteristic current. The high magnitude of field current may threat to demagnetize rotor magnets, and the inverter. The duration
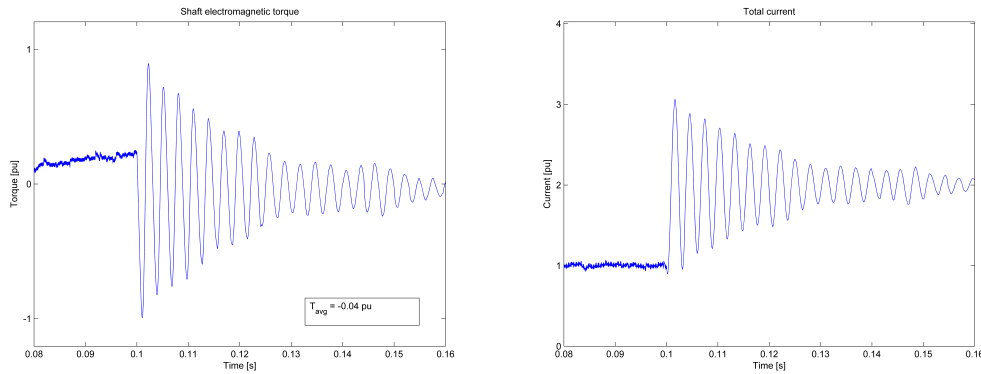
Figure 3.9: Simulation results of balanced short circuit for the simulation model. The simulation is carried out while the vehicle runs at 90 km/h. This results in a very low stationary torque, in compliance with the derived equations. Transient current reaches roughly 700 A, which is 1.6 times the characteristic current.

of the first current peak in this simulation is around 2 ms, which may be enough to thermally damage the transistor (IGBT) modules.

3.4.6 Single phase open circuit

For these simulations, the inverter continues to run, with the controller structure unaltered after the fault. For faults that are not over-lapped by inverter shutdown, the behavior after shutting down the inverter is also shown.

One switch open circuit. During operation in field weakening, one transistor fails to gate, but its integral diode is still intact.
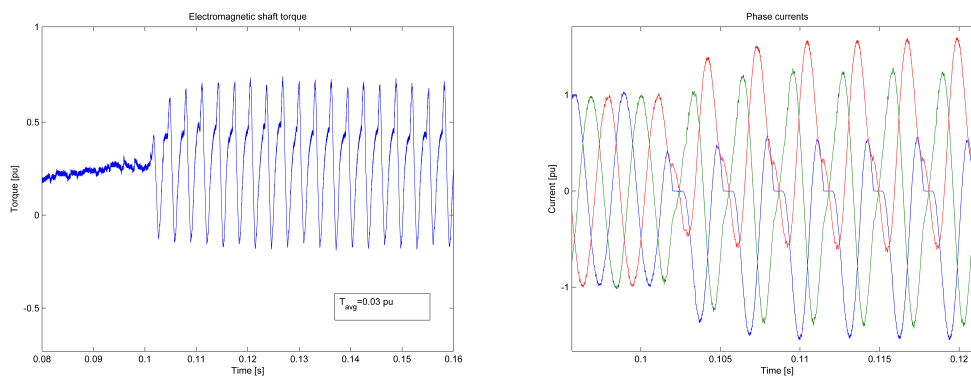
Figure 3.10: Simulation results of the one switch open circuit. Operation is continued after the fault has occurred.

Full phase open circuit In [35], the response of the IPM machine to a single phase short circuit is investigated. The results show similar behavior to the simulations for the EV model.

Both single phase open circuit faults show a benign behavior, with a low braking torque, relatively mild oscillations, and moderate fault currents. Both open circuit
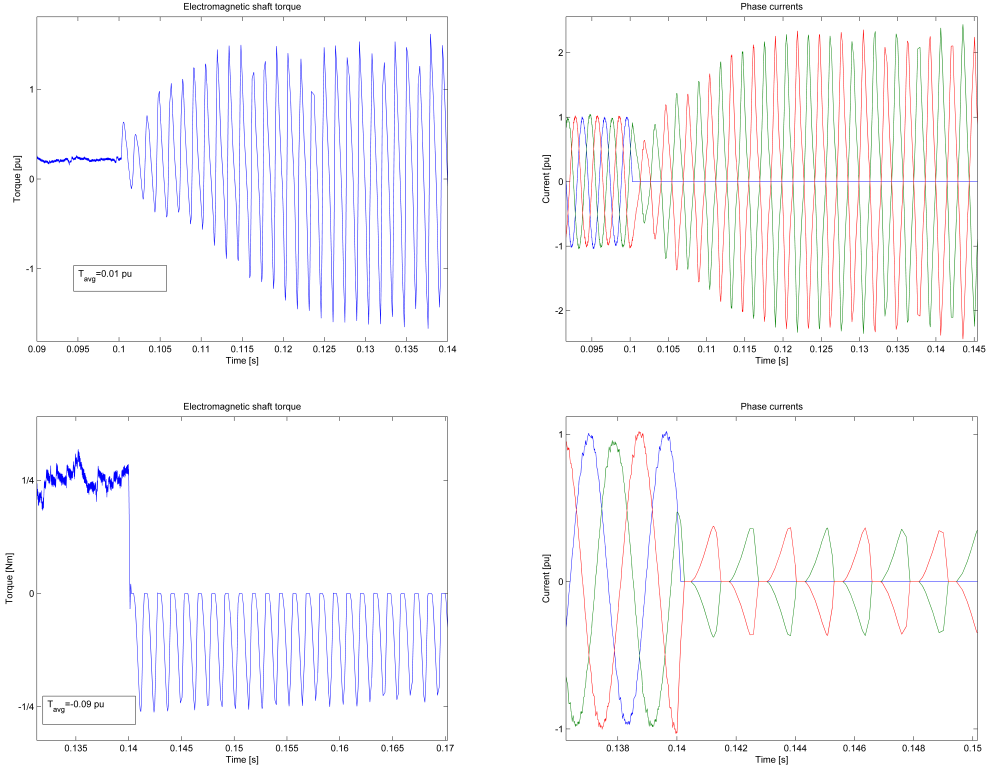
Figure 3.11: Simulation results of the one phase open circuit. With continued operation (top), and after inverter shutdown (bottom).

fault do not provide torque enough to propel the vehicle, and the operation should be aborted.

3.4.7 Inverter shutdown

This is an important situation, because shutting down the inverter is an intuitive fault action. A thorough understanding of the high speed inverter shutdown and uncontrolled generation of PM machines may hold the key to a successful implementation. This section will treat the behavior of the inverter shutdown in it self, that is, no other faults are initiated simultaneously. Inverter shutdown may lead to uncontrolled generator behavior, which implies that the motor supplies energy to the DC link via the inverter. This situation has been studied in [13, 3], and earlier by [1]. An analytic expression for the maximum braking torque is derived using some of the simplifications used in these articles and others.

A mathematical discussion of the UCG-operation is carried out in [13] and reveals some of the key behavior of this fault situation. The maximum braking torque occurs somewhere above base speed, and is asymptotically reduced at higher speed. The current rises towards the characteristic current $-\lambda_m/L_d$ as the speed increases.

Saliency has an interesting effect on UCG operation because it influences the exit point from UCG operation, and the point at which the maximum braking torque occurs. With rotor saliency greater that 2, the UCG operation is hysteretic with regard to speed. That is, a bistable region exist under the base speed, where the

motor will still generate to the DC link when the speed is reduced. For motors with significant saliency, for example IPM motors, rectifying behavior can continue down to 60% of the base speed.

Carrying out some simplifications for the inverter shutdown reveals some interesting results. It is assumed that the voltage at the DC link is constant, which implies that the battery is able to absorb all the braking power. The validity of this simplification may be tested at a later stage, comparing the calculated braking power to the absorbing ability of the battery. In [3], and later in [18], it was shown that the constant-voltage rectifier fed by a synchronous machine, under continuous conduction, can be simplified to a series balanced resistance. A short presentation of the applied derivations is carried out in the appendix (section B.3).

Simplifying the inverter to a series resistance is useful because it allows the usage of the equations derived for the balanced three phase short, by adding the inverter model resistance to the stator resistance. Particularly interesting is that the maximum torque is independent of the resistance (eq. B.11 and section 3.4.5). The resistance added by the inverter acts to shift the maximum braking torque to a higher speed. For non-salient machines, using the expression for the equivalent resistance (section B.3) and equation 3.8, the speed at which the maximum torque occurs is calculated to (see section B.3):

$$\omega_{max-torque-UCG} = \underbrace{\frac{R_s}{L_s}}_{stator\ resistance} + \underbrace{2\sqrt{2}\frac{V_{dc}}{\pi\lambda_m}}_{inverter\ voltage} \tag{3.10}$$

The terms can be split into one term caused by the stator resistance, and one caused by the inverter. For the EV model machine, approximating the L_s inductance to L_d gives that the max torque should occur at 102 km/h.

These simplifications leads to the expectation that the maximum braking torque under inverter shutdown should be nearly the same as for the balanced three phase short circuit. This proved to fit the simulation well. The vehicle simulation is carried out by gating off all transistors while the motor runs at 90 km/h.
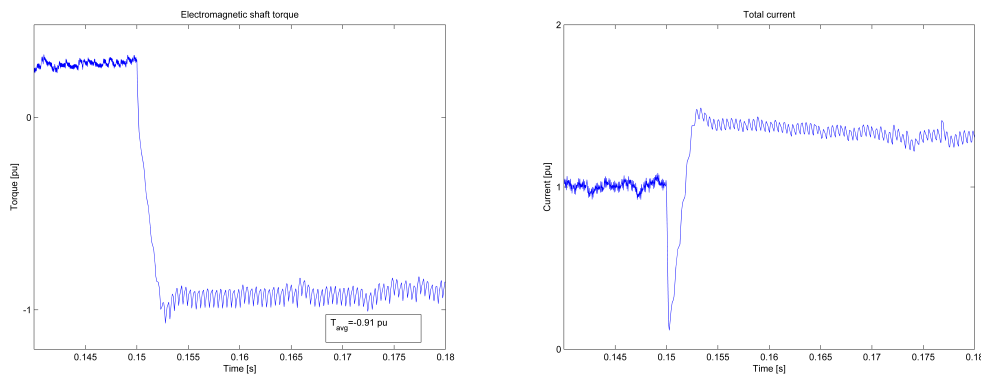

Figure 3.12: Simulation results of the inverter shutdown. The high braking torque exceeds the average braking torque simulated for any other fault.

The simulation results in figure 3.12, reveal a braking torque of around 75 Nm,

which is very near the calculated braking torque of 77 Nm calculated for the balanced short for this machine. Another simulation was done to find the braking torque at different speeds. For comparison, this simulation was also carried out by assuming that $L_q = L_d$. The results are depicted in figure 3.13.
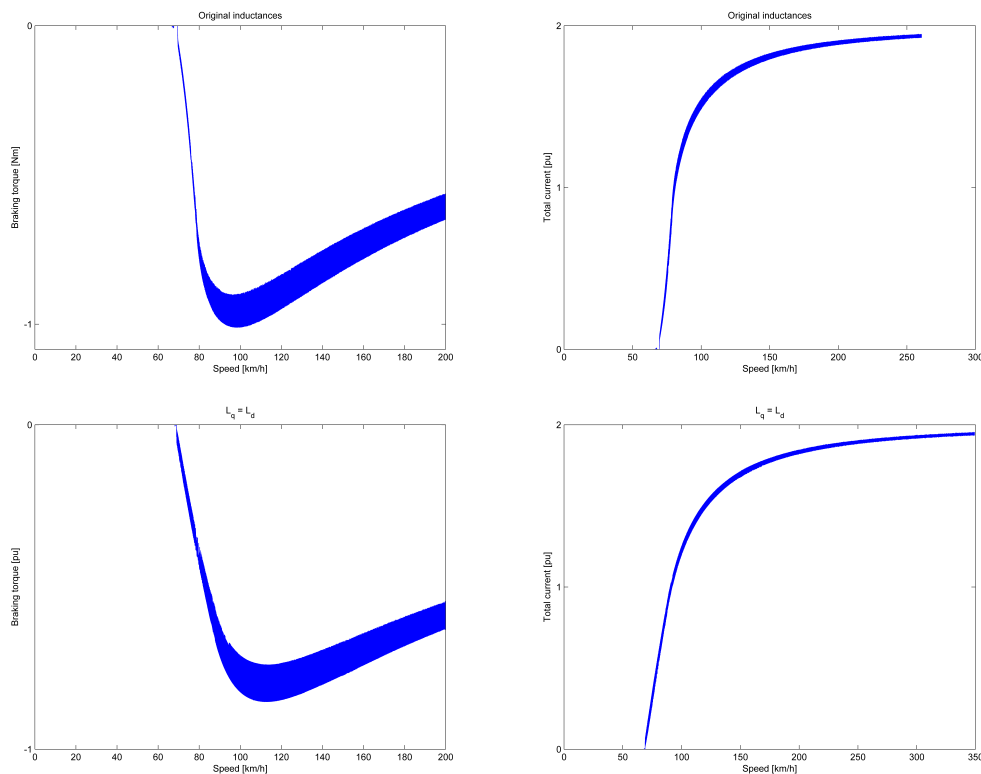
Figure 3.13: Uncontrolled generation behavior for the original machine and the machine with $L_q = L_d$. Although the machine with $L_q = L_d$ has a lower total inductance, it shows a lower braking torque than the original salient machine.

The resulting maximum torque and the speed at which it occurs agrees well with the derived values using equation B.11 and 3.10. Differentiating the equation for the maximum braking torque, assuming a given value of L_d, reveals the result that a non-salient machine will have the lowest maximum braking torque under otherwise equal conditions.

The braking torque of the EV motor, around 75 Nm, is relatively high compared to the maximum stationary torque of 80 Nm. This is the highest stationary braking torque simulated for any fault situation. It should be noted that both the current and torque is less fluctuating under inverter shutdown than what was calculated under the balanced short. Two possible reasons can be pointed out: a higher resistance will act as a damping factor in an R-L-EMF series circuit. Secondly, the rectifier only allows current to flow in one direction (from the machine), which may also have some damping effect. A simulation done later in section 4.2.1.1, indicates that the latter effect is small.

The generating behavior was partly analyzed assuming a constant DC link voltage. This simulation, however, shows the highest rise in DC link voltage. Using the transient battery model, the increase in DC link voltage is about 60 V at maximum

speed. Calculating the braking power by $P = \omega T$, the braking power at 120 km/h is roughly 110 kW. Although below the overload power, the battery may not be able to absorb this power, which would result in a possible destructive voltage rise.

3.5   Some end remarks

From this simulations, and the results from [32], it appears that the d-axis current is most prominent during short circuit faults and UCG behavior. This may qualitatively be explained realizing that the back EMF lies in the q-axis, and that the stator impedance is almost purely inductive. Because of motoring convention, current that occurs when the EMF supplies the motor inductance, is negative. This has some consequences that are worth noting;

- Strong saliency will have a significant influence on faulted behavior. This was already shown in section 3.4.1.

- Currents occurring during faults pose a risk of demagnetizing permanent magnets.

- The L_d inductance reduces the occurring currents under faults.

Among all the simulations, the maximal braking torque occurred under the inverter shutdown. The torque fluctuations of faults like the single switch short is likely to pose serious mechanical stress, but the average torque is not very high.

3.5.1   Energy absorbing potential

For serious faults like short circuits, the exact faulted behavior is difficult to predict, especially because the involvement of the fault is uncertain. Seen from the wheels, a braking torque, or more correctly a braking power, must be the result of energy being absorbed somewhere. Energy can be absorbed by energy storing devices such as the battery and (super-) capacitor, or through heat in the machine or inverter.

Chapter 4

Fault mitigation techniques presentation

There are several ways to interrupt or mitigate faults in permanent magnet machines. They may even be equipped with an ability to "limp home" after suffering from a fault. However, many of these methods have implications on cost and performance. The goal of this chapter is to concisely present some of the interesting methods that exist for fault handling. Also included shall be a discussion on which faults that are handled by the fault, what requirements that exist for the motor and inverter.

4.1 Introduction

Some faults have been introduced in chapter 3. The goal of this chapter will be to introduce concepts of fault mitigation and fault handling from the literature, and identify for which faults these methods actually provide protection of gear and passengers. Further, it will also be interesting to know what additional parts and design features that have to be adopted. There are various articles targeting fault tolerant operation and topologies. How to detect faults for the respective fault handling strategy will also be addressed in this chapter.

Fault mitigation methods may be divided into passive and active types. Passive fault handling measures are applied once, and require no additional control of the inverter after the fault. Active fault measures typically control the voltage on the terminals to counteract the fault, or even operate the motor with the fault present.

Since sensor faults are viewed as a separate family of faults, and their handling differs from direct faults in the hardware, they are addressed separately.

Later, based on this chapter and on chapter 3, suggestions to fault mitigation will be made.

4.2 Passive fault handling strategies

Passive fault handling strategies only require the determination that a fault has occurred, and for all types of fault (sensor faults excluded), the same simple action is taken. The passive methods addressed here, is the inverter shutdown and the balanced three phase short circuit. Both of these fault measures require no additional parts.

4.2.1 Inverter shutdown after a fault

Simply shutting down the inverter is an intuitive action after a fault. It implies that the motor will work as an uncontrolled generator if the fault occurs above base speed. The behavior of the inverter shutdown is shown in the section on faulted behavior (section 3.4), since for all short circuit simulations, the inverter has been passivated. For open circuit faults, passivating the inverter will result in a pure symmetrical inverter shutdown, except in the case of the true open circuit. This case was shown with and without continued operation.

The switch short circuit show a concerning behavior after the inverter shutdown. However, the shorted switch will likely not be able to handle the short circuit very long, and if the shorted switch burns out in a well behaved fashion, this situation will correspond to the inverter shutdown or full phase open circuit. A shorted switch will most likely not have the energy absorbing capability to cause much braking power.

Pure inverter shutdown, that is, inverter shutdown under otherwise healthy condition, seems to produce a high braking torque when applied at high speed. This torque can be adjusted by eq. B.11 (or 3.9 for non-salient machines).

Short circuits in the machine have a lager energy absorbing potential. When the inverter shutdown is applied, little current flows in the machine, which can make short circuits in the machine evolve rapidly.

4.2.1.1 Inverter shutdown with adjustable DC link voltage

If the DC link voltage could be adjusted to fit the stator voltage during inverter shutdown, no power would be transferred to the battery/DC link. Adjusting the DC link voltage will also increase the constant torque region, as commented in section 2.3.1. In UCG-operation, since the maximum torque occurs around base speed and maximum current rapidly rises, the maximum DC link voltage would have to exceed the maximum back EMF. If not, the maximum braking torque would only be shifted to a higher speed, implying an even higher braking power.

Actually, shifting the voltage down at the DC link during faults may be as interesting as shifting it upwards. Lowering the DC link voltage under faults would shift the speed of the maximum braking torque to a lower speed. Motivated by the assumption that the rectifying behavior by the inverter may damp the transient behavior, a simulation was carried out where the DC link was shorted after the fault: The result is shown in figure 4.1. As seen, the transient is near identical to the case
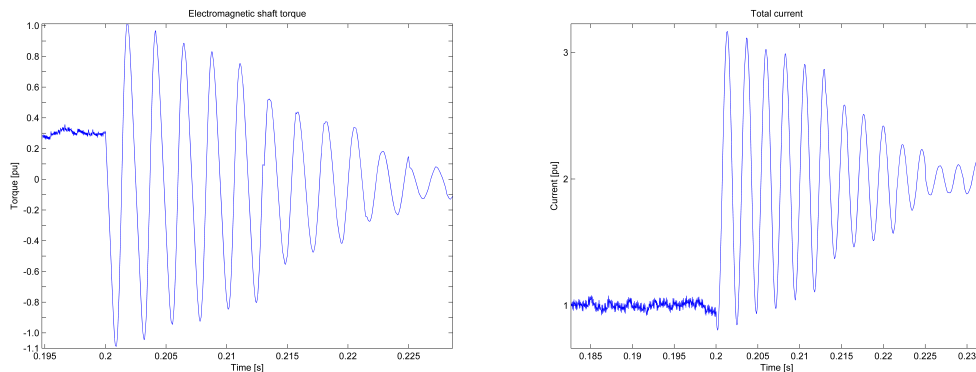
Figure 4.1: Simulation after shorting the DC link while running at 100 km/h. The result corresponds to the case balanced short, which indicates that rectification of the currents does not damp the transient as much as the DC link voltage after inverter shutdown.

of the balanced short. This indicates that it is the voltage at the DC link that is the most prominent in damping the transient during inverter shutdown.

4.2.2 Balanced three phase short

The balanced short was suggested as a fault measure in [21]. The balanced short circuit may mitigate turn-turn and machine shorts better than the inverter shutdown. Depending on the mutual inductance between the full winding and the shorted turns, the flowing current will act to depress the short circuit current in the faulted phase [10, 21].

With the 3-bridge, 3-phase inverter, a balanced short circuit can be applied by gating on the ppp or nnn transistors simultaneously. Since two possibilities exist to apply the short, it may also be applied after any single switch fault in the inverter. According to theoretic and empiric suggestions presented in 3.4.5, the current will monotonically approach the asymptote of the characteristic current $-\lambda_m/L_d$ for increasing speeds.

The full phase open circuit is not well mitigated using this method, as it imposes an unbalanced two-phase short to the machine terminals. This was pointed out in [35], and the same result may be realized in the EV model. The results shown in figure 4.2 indicate that this fault is not well covered by this fault strategy. Compared to shutting down the inverter after this fault, the balanced short has little advantage.

Looking at fault simulations, and research results of [32], it also seems that the balanced short can have a significant transient behavior. This might not be concerning regarding the torque, because it will probably be quite effectively damped out. However, even short current peaks may destroy the inverter switches, because of the low thermal inertia of power electronics. For this reason, power electronic switches may need to be rated for approximately twice the characteristic current in order to survive the balanced short.
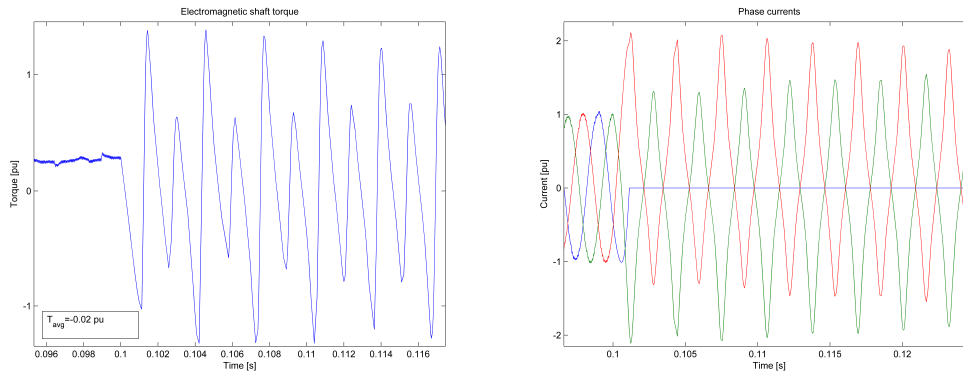
Figure 4.2: Balanced short as fault measure to full phase open circuit. May be compared to figure 3.11, where the inverter i shut down after the fault.

4.3 Active fault handling strategies

These fault handling methods have an increased part-count and require specifically adopted fault handling control strategies in the event of a fault. The presentation will be limited to motors that have 3 phases, but can easily be transferred to motors with a higher number of phases.

Because all of these methods use the remaining (two) phases to counteract the fault, they all require the ability to abort the influence of the fault, and to have some degree of freedom to control the current in the remaining phases.

4.3.1 Fault isolation

Fault isolation is done to minimize the influence of the faulted phase, and is relevant when continued operation is wanted. In general, two basic methods are presented to isolate the faulted phase. Phase isolation may be done by imposing an open circuit to the phase terminal . This can be done by adding back-to-back thyristors in series with each of the motor phases [31]. This is preferred over fuses, since fuses cannot be controlled. The thyristors will need to have an increased voltage rating to handle the full EMF from the motor. The thyristors will act like a breaker, that cuts the current at the subsequent zero crossing after the fault has been detected.

A second fault handling measure is to fully shorten the faulted phase, a strategy suggested for fault tolerant machines because it also covers short circuit faults [40]. The shorted phase must not interfere with the healthy phases, which require the machine to have very little mutual inductance. In addition, the faulted phase must be able to handle the short circuit current continuously. Imposing the short circuit can be done by having individual H-bridges for all phases, or by using two 3 phase inverters (for 3 phase machines). For both of these topologies, two ways of shortening the faulted phase exist, either by gating both upper or lower transistors of one phase.

4.3.2 Fault tolerant inverter

For faults occurring in the inverter, redundant inverter topologies exist that replaces the faulted part by altering the configuration and using redundant parts. Fault tolerant inverters are presented in [2].

In [2] and [29], an inverter topology having four poles, the fourth connected to the neutral point (star connected), is presented. The inverter can continue to operate the motor after any single short or open circuit in the inverter. The inverter needs to have the ability to fully isolate the faulted phase, and this is done using back-to-back thyristors or fuses.

Using this inverter topology, torque can be produced after a fault occurring in one phase. However, the additional volt-ampere rating is larger than for the flux-nulling six-legged inverter. This is because of the many appliances needed to fully isolate the faulted phase.

4.3.3 Flux-nulling

It has been theoretically and experimentally demonstrated that it is possible to null the flux linkage in a faulted phase using the remaining two phases after a short circuit fault [34, 30]. This will minimize the current in the faulted phase. Using individual h-bridges or two cascaded 3-phase inverters, the faulted phase is shorted in the event of a fault, and the two other phases are given current references to null the flux in the faulted phase. The inverter consists of six legs, but the volt-ampere rating of the silicon is only increased by 15%, compared to the conventional 3 phase inverter. This is because with this topology, the full DC link voltage may be utilized over all the phases. This also implies that a different voltage rating may have to be used for the motor.

In addition to minimizing the fault current, this method also imply a very low faulted torque, since the q component current is controlled to be zero. In order to fully null the flux linkage, a current of amplitude $\sqrt{3} \cdot (\lambda_m/L_d)$ needs to be supplied to the remaining phases. A zero-component current is used together with the d component current. This also requires a zero current path to exist in the topology, for example by paralleling two three phase inverters to the same battery (see figure 4.3).

Another flux nulling method that results in a very low braking torque use only d axis current. This method will not minimize the current in the faulted phase, but limit the phase currents to λ_m/L_d. It is similar to the three phase short circuit, but differs in that it produces a lower braking torque.

4.3.4 Continued operation

It is possible to create a rotating magnetic field using only two phases in a three phase machine. Hence, torque can be produced by the two remaining phases after a fault. This requires however, that the fault situation can be sustained. Interrupting the fault situation by either imposing an open or a short circuit imply extra cost
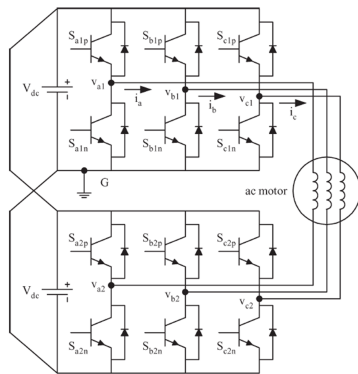
Figure 4.3: Inverter topology to null the magnetic flux (fig. from [34])

and additional parts to the inverter. Short circuit faults occurring in the machine are difficult to interrupt into open circuit faults. For instance will the inter-turn short circuit continue to produce heat if the phase terminal is disconnected. Fault tolerant machines exist that, in the event of a fault, shortens the infected phase [39]. This however, will require that the short circuit current can be sustained in the faulted phase, and that the shorted phase has a very low influence on the other phases. These are strong requirements on the design of the machine.
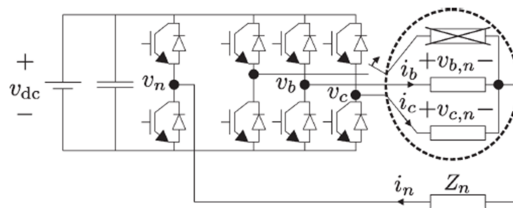
Figure 4.4: Minimal inverter topology for continued operation. From [29].

One of the simpler fault tolerant arrangements, covering inverter faults and open circuit faults in the machine, consist of currents can be controlled relatively (to be explained) independent in the the two remaining phases, the torque of faulty phase action can be nulled out in the event of a short circuited phase. Having the ability to control the neutral voltage by attaching it to a fourth inverter leg is sufficient [28]. A presentation of a topology with individual three phase rectifiers for all phases is made in [17].

4.4 Sensor faults

In [15], a fault tolerant controller that can continue to operate after a fault in any sensor is presented. The proposed drive contains a position sensor, a DC link voltage sensor and current sensors.

Sensor-less operation allows the motor to work without the speed or angle sensor. Two main methods exist to observe the rotor position electrically. The back EMF can be used when the rotor is in motion. At low speed, high frequency injection of

voltage can be used, at least if the motor has saliency. With saliency, the inductance varies along the rotor periphery, which makes the current response depend on the rotor position.

At least two current sensors are normally equipped in the drive configuration. If one current sensor fails, the other currents may be observed by a closed loop observer. If both (or all) current sensors fail, a feed-forward observer from the voltage can be used to observe the current. Because no means to observe mechanical disturbance (torque) exist, fault in current sensors will significantly reduce the dynamics of the controls.

4.5 Fault detection and diagnosis

In order to take action in fault situations, faults must be detected. In the field of fault detection and diagnosis, the following terminology is often used [6]:

1. *Fault detection* is the the general decision made by the detection unit, that a fault has occurred.

2. *Fault isolation* refers to the identification of the fault location - narrowed down to the part which is faulted.

3. *Fault identification* describes magnitude of the fault further.

It is obvious that more information is needed for more specific fault strategies. For the pure passive mitigation methods, the only requirement is that faults must be accurately and quickly detected (fault detection). For the active mitigation techniques, information regarding what phase that has been damaged is needed (fault isolation). Combining the passive fault handling based on the type of fault will require, in addition to fault detection, a classification of the fault.

The ideal fault detection strategy will add no measuring components apart from the ones needed by the current controller. Faults in measuring devices should also be detected.

In general, two different approaches to fault detection exist [6], both may be used for PM machines. The division is made into detection methods that use the mathematical model of the system, and ones that do not use the mathematical model of the system.

The most relevant method among the *Model-Free methods* is the spectrum analysis. Some type of faults have typical impacts on the harmonic contents of the current. Analyzing the current spectrum can therefore help to identify faults.

Model-Based methods are based on observers, and have been firmly established since the introduction of the Kalman filter (observer) in 1989. Observers use a mathematical model and the measurements to estimate the states of the system. Requirements exist to the observability of the system, but this is beyond the scope of this thesis.
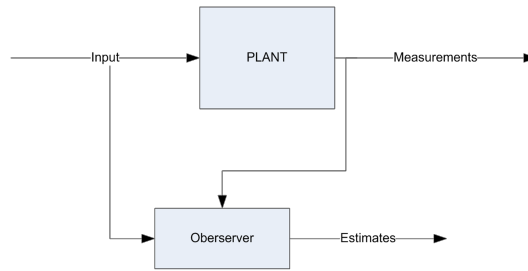
Figure 4.5: The principle of the observer. The inputs and measurements are used to estimate the states of the system.

Because of the existence of complex non-linearities and uncertainties, especially determining L_q and R_s, using *Model-Based methods* is difficult for permanent magnet machines [19]. The article ([19]) presents a method to observe L_q and R_s in order to have an accurate model for fault diagnosis. In model-based methods, a comparison between measured values and model values is made. Based on the comparison, a residual is generated. Fault determination is based on this residual which ideally should be zero in non faulty conditions, and non zero when a fault exist. A more accurate mathematical model will make the quality of the fault determination better.

Motor faults. The intra-winding (turn-to-turn) short circuit should be detected at an early stage to minimize local heating. Detecting intra-winding short circuits has been thoroughly investigated for induction machines, and some publications regarding PM machines also exist.

Detection of winding shorts have been investigated in [9], where the fault is detected realizing that the inra-winding short circuit will affect the time constant of the voltage to current transfer function. Therefore, the controlled current compared to the reference signal is used to determine a shorted turn. This method however, does not work at low speeds and loads. For these operation conditions, a high frequent current peak is demanded and the response measured.

The harmonic content of the stator currents is investigated in [24]. It is argued that the harmonic content of the current can be used to identify short circuits between turns, and experimental results for different machines at different speeds support this method.

Inverter faults. Inverter and sensor faults are considered in [23], where the shape of the current locus in the stationary dq reference frame is analyzed. For inverter faults, the locus will deviate significantly from the circular motion under sinusoidal currents. This method accurately determines the type of fault and the faulted transistor.

Sensor faults. In [15], methods to observe sensor faults are presented. They are shortly reviewed here.
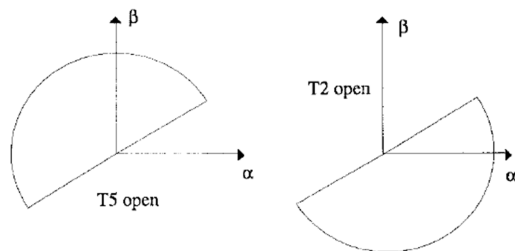
Figure 4.6: Current trajectory in the stationary dq coordinate system under two inverter switch open circuit faults. From [23].

Encoder/resolver   A fault in the encoder/resolver, or position sensor, is observed through a comparison between a parallel observer and the sensor output. If the difference between the sensor and observer exceeds a determined tolerance, the drive turns to sensor-less control. Sensorless determination of the rotor angle can be done using information from the back EMF when the speed is high enough. At low speeds, using a motor with saliency, the rotor position can be approximated using high frequency current injection.

DC-link voltage   Using an approximation of the power balance in the drive train reveals a fault in the DC link voltage sensor. Without a DC link voltage sensor, control algorithms need to be adjusted for higher stability, since DC link voltage fluctuations cannot be observed [15].

Current sensor   Current sensor faults may be determined through a comparison between the two current sensors. A short test (25 ms) can be carried out, where one of the phases are left out. If the voltage is applied correctly, the measured current should be the same in both current sensors, and deviations implies that one sensor malfunctions.

Figure 4.7: A topology implemented by the inverter to test the current sensors. In this circuit, the current sensors should measure the same value. Figure from [15].

Chapter 5

Feasible fault handling for vehicle traction

So far, machine design, faulted behavior and methods for mitigating faults have been described. The following chapter will discuss implementation of fault handling strategies, and suggest design requirements.
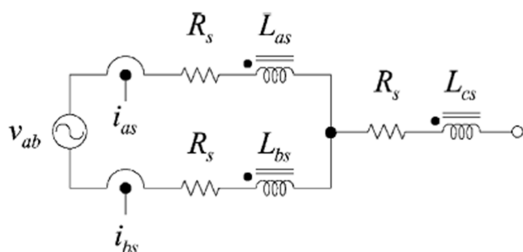
5.1 Design presumptions and suggestions

Vehicle traction does not strictly require the ability to continue operation after a fault. While this ability must be insured in crucial systems such as steer-by-wire, passenger safety is insured as long as the vehicle may be brought safely to rest. This will, at least, not be different to the behavior of vehicles today.

The ability to continue operation after all types of faults has major implications on the motor and inverter design (see design in [40]). Continued operation after open circuit faults is less design restrictive, and can be accomplished by fault isolation and adding voltage control to the neutral point.

It is not expected that the vehicle may continue normal operation after a fault even if the drive is designed to limp home, so a workshop inspection would in any case be necessary. In addition to the increased cost of more complex topologies, they are less reliable. The required inverter for flux-nulling capability is expected to be roughly 15% more expensive than the standard inverter, which may be much in a cost sensitive business.

Increasing the base speed using a DC link boost capacitor has also been addressed. The boost converter will contribute to the weight and add extra parts to the drive train. In addition, to gain the wanted fault protection by lifting the base speed during faults, the highest DC link voltage would have to be substantial.

This presumption of a standard inverter will put restrictions on the design of the drive system, especially related to the fault handling strategy.

5.1.1 Fault handling

Based on the suggestion that a minimal inverter structure will be used, two fault handling strategies are suggested and will be compared, namely the two passive fault handling strategies. In both of these methods, the faulted steady state current rapidly rises towards the characteristic current as the speed increases and if no other more serious fault is present.

The balanced short has a lower steady state braking torque at high speed, and may "over lap" several of the serious short circuit faults. Once the balanced short is applied, braking power comes from conduction losses in power electronics and conductors. One of its main concern is the transient behavior, where currents up to twice the characteristic current is demonstrated in [32] (1.6 times for the EV model). The balanced short does not cover the true open circuit well; this fault is better mitigated by the inverter shutdown.

The inverter shutdown may be interpreted as an off-set form of the balanced short circuit. The maximum torque is nearly the same, but the speed at which the maximum braking torque occurs is approximately off-set by $2\sqrt{2}\frac{V_{dc}}{\pi\lambda_m}$. Both simulation results and a similar experiment in [13] suggest that the inverter shutdown has less oscillating torques and currents than the balanced short. Simulation results in this thesis indicate that this is mainly due to the damping effect by the voltage at the DC link.

As pointed out in 3.3.2, the largest share of short circuits in the motor are expected to have been initiated by a short circuit between winding turns. Faults that may follow from intra-winding shorts include up to full phase short circuit and short circuits between phases. Both of these faults may exhibit serious faulted behavior, so an early detection and counteraction would be advantageous. Relieving this type of fault will probably be most effective if current is allowed to flow in the remainder of the phase, so that the mutual inductance to the rest of the winding will act to depress the current in the shorted turn.

Open circuit faults, though not as serious as the short circuit faults, are also expected to be a relatively frequent fault type. These faults are well covered by shutting down the inverter, given that the braking torque is tolerable.

A voltage rise on the DC link will follow after high speed inverter shutdown. The battery of the EV simulation model was able to clamp the voltage to approximately 380 V under high speed inverter shutdown, which was the simulation that showed the highest voltage rise. Since ratings of modern IGBT modules start at 600 V, this rise in voltage is not expected to damage the inverter. The ability of the battery to absorb the braking power during faults must be addressed to limit voltage rise at the DC link.

To sum up, both methods have their strengths and drawbacks. A combination of the methods, where the balanced short is applied for short circuit faults, and the inverter shutdown for open circuit faults, could be a solution. However, this will require that both the design requirements of the balanced short (transient) and the inverter shutdown (braking torque) must be addressed simultaneously.

5.1.2 Braking torque during inverter shutdown

For the EV model, the braking torque during inverter shutdown was high. This concern led to the examination of the behavior of the torque during such operation.

Analytical equations have been presented for the maximum torque under inverter shutdown, and the speed at which it occurs. The equations have been derived using simplifications from the literature, and proved to fit the simulation model well. Their validity also proved to be good when varying design parameters in the simulation model. The equations have nonetheless not been tested in practice. Depending on their usefulness, they may be good design tools to limit the amount of braking torque during high speed inverter shutdown.

The maximum braking torque for a non-salient machine was calculated to $-\frac{3}{4}\lambda_m^2\frac{n_p}{L_s}$. Reducing the flux linkage has the highest influence on the braking torque, while an increased inductance also lowers the braking torque.

5.1.3 D-Axis current and transient during balanced short

During balanced short, current peaks during transient was high. To apply the balanced short circuit, the inverter needs to be rated to handle these transients. The inconvenience of this depends on the amount of wanted overload torque. In an optimal design, the requirement of torque during overload, and the faulted current should be in the same area.

The high amount of current can damage the permanent magnets of the motor, a concern also commented in [32]. A s-axis current above the characteristic current is especially concerning, because it will invert the direction of the air gap flux. Although demagnetization is not a threat to passengers, the motor may be an expensive part to replace if the balanced short is imposed for a much less severe and frequent fault than a motor fault.

Early papers investigated the terminal short behavior of PM machines, and found that modern magnets can sustain relatively large short circuit currents without suffering from demagnetization [26]. The interior PM machine is less susceptible to demagnetization under high current, because the magnets are better protected. Especially in surface permanent magnet machines, attention should be given to avoid demagnetization under balanced short.

5.2 Faulted current and overload capability

It is clear that choosing the right PM motor for vehicle traction is a process that invoke many trade-offs. A high flux linkage gives much torque per amount of current, but aggravates the faulted currents and torque. A high inductance limits the faulted current, but requires more reactive power to be supplied to the machine.

A tractable solution would be to chose overload capability in the magnitude of the current that occurs during the majority of faults. Since the characteristic current λ_m/L_d occurs in both the inverter shutdown and steady state balanced short, this

could be chosen as the minimum overload capacity. This suggestion was also made in [21]. Applying the balanced short, the rating might have to be increased even more. The motor should be thermally capable of withstanding the increased temperature produced by the characteristic current, for the time that it takes to stop the vehicle.

This is not an as heavy design restriction as requiring $I_{rated} = \lambda_m/L_d$, which is the requirement in fault tolerant machines. For instance, the vehicle motor chosen for the design simulations had a characteristic current of 2 times the rated current. Fitting the inverter to handle this current made up to roughly 150 Nm of torque available for short time periods.

The characteristic current is determined by the d axis inductance L_d, and the flux linkage λ_m. For most types of salient PM machines, since the magnets lie in the d-axis, L_d will be smaller than L_q. The negative saliency implies that negative d-current contribute to a reluctance torque, which is favorable during operation, especially if the motor is expected to work much in field weakening operation. However, a high inductance can degrade the general performance.

The phasor diagrams of figure 5.1 illustrate that more voltage is needed when the inductance increase. Another effect caused by a high inductance is that the current dynamics are slowed because of the increased time constant.
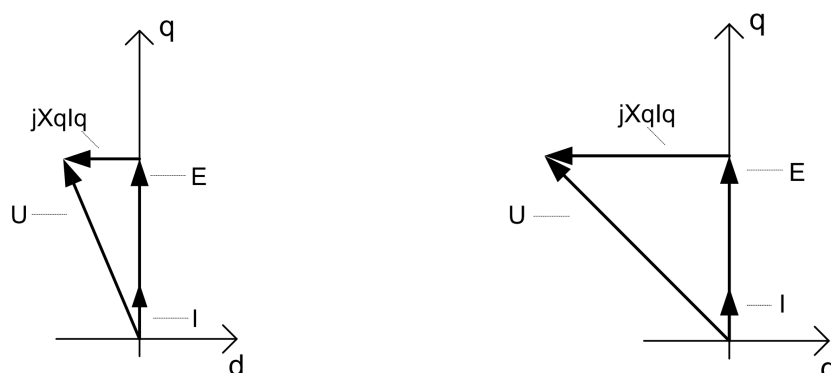
Figure 5.1: Phasor diagram using only q axis current. The inductance in the figure to the left is lowest. Note that a higher voltage is needed to supply reactive power to the machine to the right. Also note that the inductance in this situation is the q axis inductance.

Positive salient machines, for example flux concentrating (radial mounted) permanent magnet machines have a low q axis inductance and a high d axis inductance. Using this design may therefore be favorable when designing the inverter to withstand the characteristic current. No reluctance component can be utilized with this type of machine, but, with a high L_d inductance, field weakening will require less current.

5.3 Faults striking multiple phases

Short circuit faults may occur between phases. There are many different combinations of faults possible, ranging from the terminal short circuit to short circuits

near the neutral point. The effectiveness of the mitigation methods is difficult to discuss for these types of fault. In the literature, fault tolerant arrangements seem to include full phase separation in the motor, in order to make this fault very unlikely. Faulted behavior of inter phase short circuits seems to be an area where few publications exist. Distributed winding arrangements often over lap to reduce air gap field harmonics. Therefore, coils from different phases often share the same slot in a machine.

In order to simulate these types of fault in a satisfactory manner, more advanced models are needed. It is difficult to make a conclusion whether PM motors for traction purposes should have phase separation or not.

5.4 Special concerns in vehicles with multiple motors

Electric vehicles may have multiple motors. Vehicles that are equipped with multiple motors have a degree of inherent redundancy. If one motor fails, the others could in theory continue to operate and propelled the vehicle. The behavior of the faulted motor, however, needs to be addressed to produce a rational driving performance. The remaining motors can be used to compensate for the fault torque in the failed motor. It is expected that this compensation will be much simpler if the faulted behavior is stable and the fault torque is low.

The quite considerable braking that may follow from inverter shutdown may not be desirable in multiple motor vehicles. Other, more extensive mitigation methods may therefore be required. Flux-nulling seems tractable, because it has the ability to produce very low fault torque.

5.5 Serious faults

Using almost any fault strategy, some faults are not sustainable by the drive train. Serious faults, although they may be a damage to inverter, battery, motor or mechanical parts, may still be safe for passengers. If faults are relatively rare, the economically feasible solution may very well imply that components are destroyed. High currents may cause the inverter to burn out, and high oscillating torques can cause the gear or other mechanical devices to fail.

In the simulations, no fault had an average braking that exeeded that of the inverter shutdown. This can quantitatively be explained by the energy absorbing capability of the battery, which may recieve high amouts of power during this situation.

The simulations done in this thesis was only carried out to be coarse indications of the faulted behaviour. More design spesific or even laboratory tests should be carried out to further examine faulted behaviour, escpecially of faults that have the potential of absorbing much power (eq. motor short circuits).

Chapter 6

Conclusion

This thesis has studied implementation of PM motors in vehicles assuming that their implementation is tractable due to a low weight and high compactness.

For traction purposes, the ability to continue operation after an occurring fault is not absolutely necessary. Fault tolerant arrangements impose an increased cost to inverter and the machine. Because of the high cost sensitivity of the automotive business, increased part count arrangements are not likely to be feasible for motor traction.

During faults, passenger safety should be insured. Shutting down the inverter may be the fault action that allows the minimal current rating of the inverter. However, shutting down the inverter may result in a high braking torque. A key finding of this thesis is the mathematical result, defended by the simplifications done in [3] and [18], that the maximum braking torque of the inverter shutdown and the three phase short is nearly the same and independent of the stator resistance, namely (for the non-salient case):

$$T_{max} = -\frac{3}{4} \frac{n_p \lambda_m^2}{L_s}$$

This torque is at its lowest for a non-salient machine (assuming equal pole number n_p and flux linkage λ_m). The DC link voltage together with the stator resistance acts to shift the occurrence of the maximum torque to a higher speed. An expression for this speed has also been found;

$$\omega_{Tmax} = \underbrace{\frac{R_s}{L_s}}_{stator\ resistance} + \underbrace{2\sqrt{2}\frac{V_{dc}}{\pi \lambda_m}}_{inverter\ voltage} \approx 2\sqrt{2}\frac{V_{dc}}{\pi \lambda_m}$$

The escalation of the fault into more expensive and comprehensive faults should be prevented, especially for faults that are expected to occur relatively frequent. However, as long as safety is insured, this question will be one of cost optimization. If a fault is expected to strike very seldom, adopting measures to mitigate it in order to protect other vehicle parts, may very well not be a feasible solution to implement in all vehicles.

Intra-winding faults should be detected at an early stage. Aborting operation of

the vehicle at an early stage may prevent escalation of this fault into a more severe fault. This requires using good fault detection methods. An introduction to such methods have been carried out.

As in case of the machine model used in this thesis, λ_m/L_d could be designed to lie within normal overload conditions. The machine had a characteristic current twice the rated current, which seems a relatively sound solution. If so, the inverter will be able to handle the frequently occurring (during faults) characteristic current. Taking care during machine design, this current may very well be tolerated by the machine for limited amounts of time, both thermally and concerning demagnetization.

Saliency was shown in chapter 3 to aggravate faults significantly. During machine design, IPM machines may be designed to loose the saliency for high amounts of q-current. This may be done by actively choosing flux channel withs in the rotor, so that saturation occurs at high speeds.

Three phase balanced short	Inverter shutdown
Advantages	**Advantages**
• Expected good mitigation of short circuits	• Expected good mitigation of open circuit faults
• Low braking torque at moderate to high speed	• Need to overrate inverter limited to characteristic current.
Concerns	**Concerns**
• Increased inverter rating to handle transients	• Evolvement of (machine) short circuits
• Full open circuit fault show large oscillations	• High braking torque at high speed

Table 6.1: Summary of the comparison between balanced short and inverter shutdown.

6.1 Suggestions for further work

• Explore the transient behavior of the balanced three phase short and the inverter shutdown. Find mathematical support for the transient behavior, in order to understand the measures that have to be taken to damp it.

• Faults that occur in the machine may produce much heat power, and thereby imply a high braking torque. More advanced simulations, or perhaps laboratory test should be carried out to test the faulted behavior of machine shorts further.

References

[1] A. Adnanes, R. Nilssen, and R. Rad, "Power feed-back during controller failure in inverter fed permanent magnet synchronous motor drives with flux weakening," in *Power Electronics Specialists Conference, 1992. PESC '92 Record., 23rd Annual IEEE* (R. Nilssen, ed.), pp. 958–963 vol.2, 1992.

[2] S. Bolognani, M. Zordan, and M. Zigliotto, "Experimental fault-tolerant control of a pmsm drive," *Industrial Electronics, IEEE Transactions on*, vol. 47, no. 5, pp. 1134–1141, 2000.

[3] V. Caliskan, D. Perreault, T. Jahns, and J. Kassakian, "Analysis of three-phase rectifiers with constant-voltage loads," *Circuits and Systems I: Fundamental Theory and Applications, IEEE Transactions on [see also Circuits and Systems I: Regular Papers, IEEE Transactions on]*, vol. 50, no. 9, pp. 1220–1225, 2003.

[4] M. Ciappa and W. Fichtner, "Lifetime prediction of igbt modules for traction applications," in *Reliability Physics Symposium, 2000. Proceedings. 38th Annual 2000 IEEE International* (W. Fichtner, ed.), pp. 210–216, 2000.

[5] E. Elvestad, "Permanent magnet machine for electric vehicles," Master's thesis, Norwegian University of science and Technology, 2007.

[6] J. Gertler, *Fault detection and diagnosis in engineering systems.* New York: Marcel Dekker, 1998.

[7] J. F. Gieras and M. Wing, *Permanent Magnet Motor Technology - design and applications.* New York: Marcel Dekker, 1997.

[8] L. Harnefors, K. Pietilainen, and L. Gertmar, "Torque-maximizing field-weakening control: design, analysis, and parameter selection," *Industrial Electronics, IEEE Transactions on*, vol. 48, no. 1, pp. 161–168, 2001.

[9] J. Haylock, "On-line detection of winding short-circuits in inverter fed drives," in *Electrical Machines and Drives, 1999. Ninth International Conference on (Conf. Publ. No. 468)*, pp. 258–262, 1999.

[10] J. Haylock, B. Mecrow, A. Jack, and D. Atkinson, "Operation of fault tolerant machines with winding failures," *Energy Conversion, IEEE Transaction on*, vol. 14, no. 4, pp. 1490–1495, 1999.

[11] D. Hirschmann, D. Tissen, S. Schroder, and R. De Doncker, "Reliability prediction for inverters in hybrid electrical vehicles," *Power Electronics, IEEE Transactions on*, vol. 22, no. 6, pp. 2511–2517, 2007.

[12] D. G. Holmes and T. A. Lipo, *Pulse Width Modulation for Power Converters - Principles and Practice.* Wiley Inter-Science, IEEE Press, 2003.

[13] T. Jahns and V. Caliskan, "Uncontrolled generator operation of interior pm synchronous machines following high-speed inverter shutdown," *Industry Applications, IEEE Transactions on*, vol. 35, no. 6, pp. 1347–1357, 1999.

[14] T. Jahns and W. Soong, "Pulsating torque minimization techniques for permanent magnet ac motor drives-a review," *Industrial Electronics, IEEE Transactions on*, vol. 43, no. 2, pp. 321–330, 1996.

[15] Y.-s. Jeong, S.-K. Sul, S. Schulz, and N. Patel, "Fault detection and fault-tolerant control of interior permanent-magnet motor drive system for electric vehicle," *Industry Applications, IEEE Transactions on*, vol. 41, no. 1, pp. 46–51, 2005.

[16] G. Joksimovic and J. Penman, "The detection of inter-turn short circuits in the stator windings of operating motors," *Industrial Electronics, IEEE Transactions on*, vol. 47, no. 5, pp. 1078–1084, 2000.

[17] A. Krautstrunk and P. Mutschler, "Remedial strategies for a permanent magnet synchronous motor drive," in *European Power Electronics and Drives Association*, 1999.

[18] C.-Z. Liaw, W. Soong, B. Welchko, and N. Ertugrul, "Uncontrolled generation in interior permanent-magnet machines," *Industry Applications, IEEE Transactions on*, vol. 41, no. 4, pp. 945–954, 2005.

[19] L. Liu, L. Liu, and D. Cartes, "On-line identification and robust fault diagnosis for nonlinear pmsm drives," in *American Control Conference, 2005. Proceedings of the 2005* (D. Cartes, ed.), pp. 2023–2027 vol. 3, 2005.

[20] J. Lutz, *Halbleiter-Leistungsbauelemente : Physik, Eigenschaften, Zuverlässigkeit.* Springer Verlag - Berlin, Heidelberg, 2006.

[21] P. Mellor, T. Allen, R. Ong, and Z. Rahma, "Faulted behaviour of permanent magnet electric vehicle traction drives," in *Electric Machines and Drives Conference, 2003. IEMDC'03. IEEE International*, vol. 1, pp. 554–558 vol.1, 2003.

[22] S. Nandi, H. Toliyat, and X. Li, "Condition monitoring and fault diagnosis of electrical motors-a review," *Energy Conversion, IEEE Transaction on*, vol. 20, no. 4, pp. 719–729, 2005.

[23] R. Peuget, S. Courtine, and J.-P. Rognon, "Fault detection and isolation on a pwm inverter by knowledge-based model," *Industry Applications, IEEE Transactions on*, vol. 34, no. 6, pp. 1318–1326, 1998.

[24] J. Rosero, L. Romeral, J. Cusido, A. Garcia, and J. Ortega, "On the short-circuiting fault detection in a pmsm by means of stator current transformations," in *Power Electronics Specialists Conference, 2007. PESC 2007. IEEE* (L. Romeral, ed.), pp. 1936–1941, 2007.

[25] E. Sato, "Permanent magnet synchronous motor drives for hybrid electric vehicles," *IEEJ Transactions on Electrical and Electronic Engineering*, vol. 2, no. 2, pp. 162–168, 2007.

[26] T. Sebastian and G. Slemon, "Transient torque and short circuit capabilities of variable speed permanent magnet motors," *Magnetics, IEEE Transactions on*, vol. 23, no. 5, pp. 3619–3621, 1987.

[27] A. Tuckey and D. Patterson, "A new resonant dc link/boost converter topology applied to extended speed operation of a brushless dc machine," in *Applied Power Electronics Conference and Exposition, 1998. APEC '98. Conference Proceedings 1998., Thirteenth Annual* (D. Patterson, ed.), vol. 1, pp. 294–300 vol.1, 1998.

[28] O. Wallmark, *Control of Permanent-Magnet Synchronous Machines in Automotive Applications*. PhD thesis, Chalmers University of Technology, Göteborg, Sweden, 2006.

[29] O. Wallmark, L. Harnefors, and O. Carlson, "Control algorithms for a fault-tolerant pmsm drive," *Industrial Electronics, IEEE Transactions on*, vol. 54, no. 4, pp. 1973–1980, 2007.

[30] B. A. Welchko, T. M. Jahns, and T. A. Lipo, "Short-circuit fault mitigation methods for interior pm synchronous machine drives using six-leg inverters," in *Power Electronics Specialists Conference, 2004. PESC 04. 2004 IEEE 35th Annual* (T. M. Jahns, ed.), vol. 3, pp. 2133–2139 Vol.3, 2004.

[31] B. A. Welchko, T. M. Jahns, and T. A. Lipo, "Fault interrupting methods and topologies for interior pm machine drives," *Power Electronics Letters, IEEE*, vol. 2, no. 4, pp. 139–143, 2004.

[32] B. A. Welchko, T. M. Jahns, W. L. Soong, and J. M. Nagashima, "Ipm synchronous machine drive response to symmetrical and asynunetrical short circuit faults," *Power Engineering Review, IEEE*, vol. 22, no. 10, pp. 57–57, 2002.

[33] B. A. Welchko, T. A. Lipo, T. M. Jahns, and S. E. Schulz, "Fault tolerant three-phase ac motor drive topologies: a comparison of features, cost, and limitations," *Power Electronics, IEEE Transactions on*, vol. 19, no. 4, pp. 1108–1116, 2004.

[34] B. A. Welchko, J. Wai, T. M. Jahns, and T. A. Lipo, "Magnet-flux-ing control of interior pm machine drives for improved steady-state response to short-circuit faults," *Industry Applications, IEEE Transactions on*, vol. 42, no. 1, pp. 113–120, 2006.

[35] B. Welchko, T. Jahns, and S. Hiti, "Ipm synchronous machine drive response to a single-phase open circuit fault," *Power Electronics, IEEE Transactions on*, vol. 17, no. 5, pp. 764–771, 2002.

[36] W. Yin, "Failiure mechanisms of winding insulations in inverter-fed motors," *IEEE Electrical Insulation Magazine*, vol. 13, pp. 18–23, November/December 1997.

[37] C. Chan and K. Chau, *Modern Electric Vehicle Technology*. Oxford Science Publications, 2001.

[38] A. El-Refaie and T. Jahns, "Comparison of synchronous pm machine types for wide constant-power speed range operation," in *Industry Applications Conference, 2005. Fourtieth IAS Annual Meeting. Conference Record of the 2005*, vol. 2, pp. 1015–1022 Vol. 2, 2005.

[39] A. Jack, B. Mecrow, and J. Haylock, "A comparative study of permanent magnet and switched reluctance motors for high-performance fault-tolerant applications," *Industry Applications, IEEE Transactions on*, vol. 32, no. 4, pp. 889–895, 1996.

[40] A. Jack, B. Mecrow, and C. Weiner, "Switched reluctance and permanent magnet motors suitable for vehicle drives-a comparison," in *Electric Machines and Drives, 1999. International Conference IEMD '99*, pp. 505–507, 1999.

[41] D. Patterson, "High efficiency permanent magnet drive systems for electric vehicles," in *Industrial Electronics, Control and Instrumentation, 1997. IECON 97. 23rd International Conference on*, vol. 2, pp. 391–396 vol.2, 1997.

[42] D. Patterson, C. Brice, R. Dougal, and D. Kovuri, "The "goodness" of small contemporary permanent magnet electric machines," in *Electric Machines and Drives Conference, 2003. IEMDC'03. IEEE International*, vol. 2, pp. 1195–1200, 2003.

[43] W. Soong and T. Miller, "Field-weakening performance of brushless synchronous ac motor drives," *Electric Power Applications, IEE Proceedings -*, vol. 141, no. 6, pp. 331–340, 1994.

[44] O. Wallmark, *Control of Permanent-Magnet Synchronous Machines in Automotive Applications*. PhD thesis, Chalmers University of Technology, Göteborg, Sweden, 2006.

References to the WWW

[Infineon(2008)] Infineon.   Igbt modules up to 600v dual, 2008.   URL
http://www.infineon.com/cms/en/product/channel.html?channel=ff80808112ab681d0112ab69e70c0364.

[Plexim gmbh(2008)] Plexim gmbh.   Plecs user manual, April 2008.   URL
http://www.plexim.com/files/plecsmanual.pdf.

[Tesla Motors(2008)] Tesla Motors.   Tesla roadster - technical specs, 2008.   URL
http://www.teslamotors.com/performance/tech_specs.php.

[Think Global(2008)] Think Global. Think home page, 2008. URL http://www.think.no.

[Volkswagen(2008)] Volkswagen.   Golf   technical   data,   2008.   URL
http://www.vw.no/photoalbum/view/?size=org&id=21514&type=1.

Appendix A

Definitions

A.1 Base quantities

Speed. Canceling all currents in

$$
\begin{aligned}
v_d & = R_s i_d + L_d \frac{di_d}{dt} - \omega_r L_q i_q \ , \qquad v_q = R_s i_q + L_q \frac{di_q}{dt} + \omega_r L_d i_d + \omega_r \lambda_m \\
\Rightarrow \ v_q & = \omega_r \lambda_m
\end{aligned}
$$

Defining

$$
\omega_{base} = \frac{V_{max}}{\lambda_m} = \frac{V_{dc}}{\sqrt{3}\lambda_m} \approx 1776 \text{ rad/sec} \approx 65 \text{ km/h}
$$

Currents. All currents are given with their peak values. RMS values are only used for current ratings in power electronics and motor, and is specified. The base current was chosen to the max. continious current of the motor.

$$
I_{base} = 160 \cdot \sqrt{2} \ \approx 226 \text{ A}
$$

Torque. The base torque was chosen to the maximum stationary torque under base speed:

$$
T_{base} = 83 \text{ Nm}
$$

A.2 The dq coordinate system

The space vector in the stationary stator coordinate system is calculated through Clark's transformation:

$$\underline{i}_{\alpha\beta} = i_\alpha + ji_\beta = \frac{2}{3}\left(i_a + \underline{a}i_b + \underline{a}^2 i_c\right) \tag{A.1}$$

where $\underline{a} = e^{j120^0} = -\frac{1}{2} + j\frac{\sqrt{3}}{2}$, and $i_{a,b,c}$ are line phase currents.

To transform the line currents to a rotating reference frame:

$$\underline{i}_{dq} = i_d + ji_q = \underline{i}_{\alpha\beta}e^{-j\omega_r t}$$

The same definition is used for the voltages, if the line currents are replaced by the phase to neutral voltages.

Phase currents and voltages may also be directly transferred in the rotating reference frame using the Parks transformation matrix, where also, the common mode is included;

$$\mathbf{T}_{dq} = \frac{2}{3}\begin{bmatrix} \cos(\theta) & \cos(\theta - \frac{2\pi}{3}) & \cos(\theta + \frac{2\pi}{3}) \\ -\sin(\theta - \frac{2\pi}{3}) & -\sin(\theta - \frac{2\pi}{3}) & -\sin(\theta + \frac{2\pi}{3}) \\ 1/2 & 1/2 & 1/2 \end{bmatrix}$$

e.q.

$$\mathbf{i}_{dq0} = \mathbf{i}_{ph}\mathbf{T}_{dq}$$

For symmetrical conditions, these techniques will yield the same result.

It should be noted that using this definition, the geometrical sum $\sqrt{(v,i)_d^2 + (v,i)_q^2}$ will give the *amplitude value* of the line currents or phase voltages.

Appendix B

Derivations

B.1 Maximum utilizable dq voltage

Under the assumption that the source voltages V_{az}, V_{bz}, V_{cz} in figure B.1a are balanced, $V_{zs} = 0$, i.e. the source voltages are equal to the phase voltages.

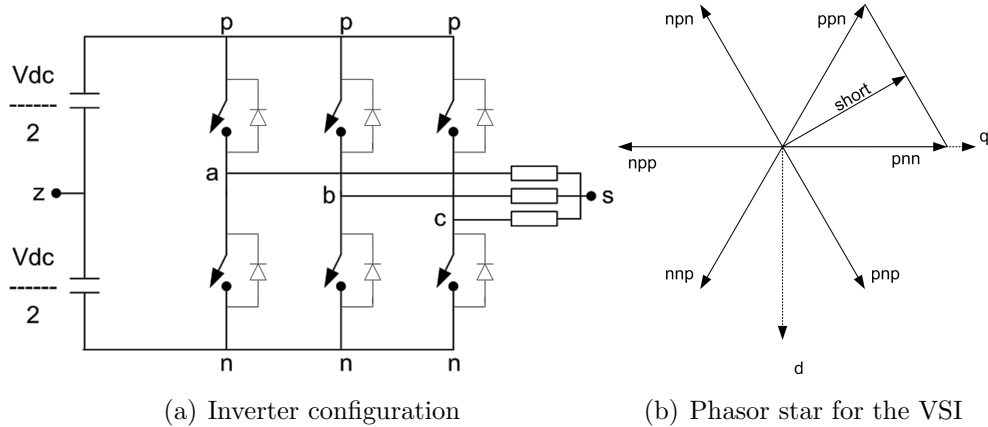(a) Inverter configuration   (b) Phasor star for the VSI

Figure B.1: Three phase inverter topology and utilizable voltage phasors in the stationary reference frame.

Using the concept of a stationary dq (or $\alpha\beta$) coordinate system, as in [12], also known as Clark's transformation (see section A.2), the different rational switch combinations can be drawn. It is assumed that each leg of the inverter has one active switch at all times.

A balanced three phase system will be a rotating phasor in the diagram in figure B.1. The length of the six stationary discrete switch states are, from equation A.1 $\frac{2}{3}V_{dc}$. To realize a phasor between two discrete phasors, PWM is adopted. The shortest phasor is marked in the figure, and is $\frac{\sqrt{3}}{2}$ times the length of the stationary vectors. Hence,

$$V_{max} = \frac{\sqrt{3}}{2} \cdot \frac{2}{3} \cdot V_{dc} = \frac{V_{dc}}{\sqrt{3}}$$

B.2 Mathematical description of the PMSM

A simulation study shall demonstrate some of the consequences of a fault. Different control regimes and means for observing the fault will also be implemented in the simulation.

The model has an accessible neutral point, which allows common mode current to flow. The derivation is a simplified version of that found in [44]. It is assumed that the flux linkages between the stator windings and the rotor magnets vary sinusoidally with rotor position:

$$\underline{\lambda}_{m,ph} = \begin{bmatrix} \lambda_m \cos(\theta) \\ \lambda_m \cos(\theta - \frac{2\pi}{3}) \\ \lambda_m \cos(\theta + \frac{2\pi}{3}) \end{bmatrix} \tag{B.1}$$

where θ is the rotor position in electrical degrees. It is further assumed that the phase self and mutual inductances vary sinusoidally or not at all (non-salient) "along" the rotor periphery. For most salient machines, the inductances vary with the double electric rotor frequency, since the reluctance repeat with each north *and* south pole.

$$L_s = L_{s,0} + L_{s,2}\cos(2\theta)$$

$$L_m = L_{m,0} + L_{m,2}\cos(2\theta)$$

$$\underline{L}_{ph} = \begin{bmatrix} L_s(\theta) & L_m(\theta + \frac{2\pi}{3}) & L_m(\theta - \frac{2\pi}{3}) \\ L_m(\theta + \frac{2\pi}{3}) & L_s(\theta - \frac{2\pi}{3}) & L_m(\theta) \\ L_m(\theta - \frac{2\pi}{3}) & L_m(\theta) & L_s(\theta + \frac{2\pi}{3}) \end{bmatrix} \tag{B.2}$$

The per phase voltage equation is:

$$\underline{v}_{ph} = \frac{d}{dt}(\underline{L}_{ph}\underline{i}_{ph} + \underline{\lambda}_{m,ph}) + R_s\underline{i}_{ph} \tag{B.3}$$

The torque developed is:

$$T_e = \frac{dW_{co}}{d\theta} = n_p(\frac{1}{2}\underline{i}_{ph}^T\frac{\partial\underline{L}_{ph}}{\partial\theta}\underline{i}_{ph} + \underline{i}_{ph}^T\frac{\partial\underline{\lambda}_{m,ph}}{\partial\theta}) \tag{B.4}$$

The phase flux linkage is:

$$\underline{\lambda}_{ph} = \underline{L}_{ph}\underline{i}_{ph} + \underline{\lambda}_{m,ph} \tag{B.5}$$

Under these assumptions a Park transformation of B.1, B.3 and B.5 gives:

$$\lambda_d = L_d i_d + \lambda_m \tag{B.6}$$

$$\lambda_q = L_q i_q \tag{B.7}$$

$$v_d = R_s i_d + \frac{d\lambda_d}{dt} - \omega_r \lambda_q \tag{B.8}$$

$$v_q = R_s i_q + \frac{d\lambda_q}{dt} + \omega_r \lambda_d \tag{B.9}$$

After carrying out the dq-decomposition of L_{ph} (eq. B.2):

$$L_d = L_{s,0} + \frac{L_{s,2}}{2} - L_{m,0} + L_{m,2}$$

$$L_q = L_{s,0} - \frac{L_{s,2}}{2} - L_{m,0} - L_{m,2}$$

Inserting eq. B.6 into B.8 and B.7 into B.9 yields:

$$v_d = R_s i_d + L_d \frac{di_d}{dt} - \omega_r L_q i_q$$

$$v_q = R_s i_q + L_q \frac{di_q}{dt} + \omega_r L_d i_d + \omega_r \lambda_m$$

Now, calculating the instantaneous power and recognizing the mechanical term gives the torque equation:

$$T_e = \frac{3}{2} n_p [\lambda_d i_q - \lambda_q i_d] = \frac{3}{2} n_p (\lambda_m + (L_d - L_q) i_d) i_q$$

B.3 Uncontrolled generation and balanced short

Differentiating the equation for the maximum torque

$$T_{e-3ph-sc} = \frac{3 n_p}{2} R_s \lambda_m^2 \left[\frac{-\omega_r}{\omega_r^2 L_d L_q + R_s^2} + (L_d - L_q) \frac{\omega_r^3 L_q}{(\omega_r^2 L_q L_d + R_s^2)^2} \right]$$

for ω_r and solving for the first order local min/max condition (derivative=0) yields four solutions, one negative, two complex, and

$$\omega_r = \frac{\sqrt{2} R_s}{2} \cdot \frac{\sqrt{L_d \left(3(L_q - L_d) + \sqrt{9(L_q^2 + L_d^2) - 14 L_q L_d} \right)}}{L_q L_d} \tag{B.10}$$

Inserting B.10 into the torque equation above yields;

$$T_{max} = \frac{\sqrt{2}}{2} 3 n_p \lambda_m^2 \frac{\sqrt{-L_d \left(-3 L_q + 3 L_d - \sqrt{9 L_q^2 - 14 L_q L_d + 9 L_d^2} \right)} L_q \left(L_d - 3 L_q - \sqrt{9 L_q^2 - 14 L_q L_d + 9 L_d^2} \right)}{L_d^2 \left(-5 L_q + 3 L_d - \sqrt{9 L_q^2 - 14 L_q L_d + 9 L_d^2} \right)^2} \tag{B.11}$$

Differentiating this equation for L_q to find the minimum braking torque results in $L_q = L_d$. The non-salient machine has the lowest possible braking torque under

inverter shutdown, under otherwise equal conditions. For a non-salient machine, the speed and torque equations simplify to

$$\omega_r = \frac{R_s}{L_d}\,, \qquad T_{max} = -\frac{3}{4}\frac{n_p \lambda_m^2}{L_d}$$

Under inverter shutdown, the maximum torque will be nearly the same, but the inverter will act as a resistance to shift the speed at which maximum braking torque occurs to a higher speed. To determine this speed, firstly, the value of the equivalent resistance needs to be found. This derivation is made assuming a non-salient machine with stator inductance L_s.

The ground harmonic voltage applied by the rectifying inverter, V_{o1}, is calculated (se fig. B.2) by

$$b_1 = \frac{1}{\pi}\int_{-\pi}^{\pi} f(x)\,\sin(x)\,dx \implies V_{o1} = \frac{2}{\pi}V_{dc}$$
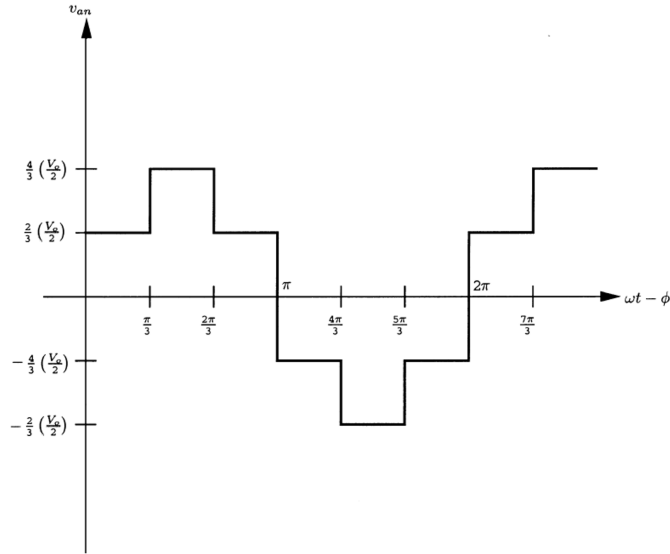

Figure B.2: Phase-to-neutral voltage seen from the machine terminals of the PMSM (from [3]). Since the back EMF is sinusoidal, only the 1st harmonic current can carry reactive power. It is expected that the current lies in phase with the machine terminal voltage. This argument leads to the simplification of this voltage form to a resistor. The magnitude of the ground harmonic voltage is $V_{o1} = \frac{2}{\pi}V_{dc}$. The value of the resistor is given in figure B.3.

Using the equation in figure B.3, replacing V_s with the back EMF $V_s = \lambda_m\omega$, and V_{o1} with the first harmonic of the block voltage in figure B.2 $V_{o1} = \frac{2}{\pi}V_{dc}$. Putting the result into the equation for the speed at which the maximum torque occurs (eq. 3.8 for a non-salient machine):

$$\omega_r = (R_s + R)/L_s$$

Using the R of figure B.3, and solving this equation for ω gives
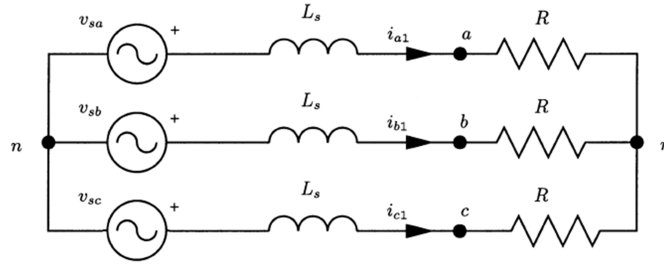
$$R = \frac{V_{o1}^2 R_s + V_{o1}\sqrt{(\omega_r L_s)^2(V_s^2 - V_{o1}^2) + R_s^2 V_s^2}}{V_s^2 - V_{o1}^2}$$

Figure B.3: Simplification of the PMSM feeding a voltage-clamped rectifier (or passive inverter) used in [3]. V_s is the magnitude of the back EMF, and V_{o1} is the magnitude of the 1st harmonic of the block voltage applied by the inverter to the machine terminals (figure B.2).

$$\omega = \frac{R_s \lambda_m \pi + 2\sqrt{2}L_s V_{dc}}{\lambda_m L_s \pi} = \underbrace{\frac{R_s}{L_s}}_{stator\ resistance} + \underbrace{2\sqrt{2}\frac{V_{dc}}{\pi \lambda_m}}_{inverter\ voltage} \approx 2\sqrt{2}\frac{V_{dc}}{\pi \lambda_m}$$

As seen in this equation, the speed caused by the inverter resistance and that caused by the inverter voltage can be split.

B.4 Closed-loop current dynamics state space model

The state space model is derived assuming an ideal inverter (i.e. $v^{ref} = v$), and inserting the controller equations into the controlled equations in section 2.5. The ideal inverter assumption can be defended as long as the modulation index is not too high, and for reasonably high switching frequencies. A well-working field weakening controller, together with a limit on speed and current references will force the controller to work within the inverter boundaries.

Inserting as described gives

$$k_{pq}(i_q^{ref} - i_q) + k_{iq}\frac{1}{s}(i_q^{ref} - i_q) + \omega_r L_d i_d - R_{aq} i_q = R_s i_q + L_q \frac{di_q}{dt} + \omega_r L_d i_d + \omega_r \lambda_m$$

$$k_{pd}(i_d^{ref} - i_d) + k_{id}\frac{1}{s}(i_d^{ref} - i_d) - \omega_r L_q i_q - R_{ad} i_d = R_s i_d + L_d \frac{di_d}{dt} - \omega_r L_q i_q$$

Defining states $\mathbf{x} = \begin{bmatrix} i_d & i_q & I_d & I_q \end{bmatrix}^T$, inputs $\mathbf{u} = \begin{bmatrix} i_d^{ref} & i_q^{ref} \end{bmatrix}^T$, and disturbances $\mathbf{v} = [\omega_r]^T$, gives the state-space system

$$\frac{di_d}{dt} = \frac{1}{L_d}\left(k_{pd}(i_d^{ref} - i_d) + k_{id}I_d - R_{ad}i_d - R_s i_d\right)$$

$$\frac{di_q}{dt} = \frac{1}{L_q}\left(k_{pq}(i_q^{ref} - i_q) + k_{iq}I_q - R_{aq}i_q - R_s i_q - \omega_r \lambda_m\right)$$

$$\frac{dI_d}{dt} = i_d^{ref} - i_d$$

$$\frac{dI_q}{dt} = i_q^{ref} - i_q$$

$$\mathbf{A} = \begin{bmatrix} -\frac{1}{L_d}(k_{pd} + R_{ad} + R_s) & 0 & \frac{1}{L_d}k_{id} & 0 \\ 0 & -\frac{1}{L_q}(k_{pq} + R_{aq} + R_s) & 0 & \frac{1}{L_q}k_{iq} \\ -1 & 0 & 0 & 0 \\ 0 & -1 & 0 & 0 \end{bmatrix}$$

$$\mathbf{B} = \begin{bmatrix} \frac{1}{L_d}k_{pd} & 0 \\ 0 & \frac{1}{L_q}k_{pq} \\ 1 & 0 \\ 0 & 1 \end{bmatrix}, \quad \mathbf{E} = \begin{bmatrix} 0 \\ -\lambda_m/L_q \\ 0 \\ 0 \end{bmatrix}$$

Now, as in [28], the controller gains are chosen so that $k_{pd} = \alpha_c L_d$, $R_{ad} = \alpha_c L_d - R_s$, $k_{id} = \alpha_c^2 L_d$. And analogous for the q-axis $k_{pq} = \alpha_c L_q$, $R_{aq} = \alpha_c L_q - R_s$, $k_{iq} = \alpha_c^2 L_q$. This yields:

$$\mathbf{A} = \begin{bmatrix} -2\alpha_c & 0 & \alpha_c^2 & 0 \\ 0 & -2\alpha_c & 0 & \alpha_c^2 \\ -1 & 0 & 0 & 0 \\ 0 & -1 & 0 & 0 \end{bmatrix}, \quad \mathbf{B} = \begin{bmatrix} \alpha_c & 0 \\ 0 & \alpha_c \\ 1 & 0 \\ 0 & 1 \end{bmatrix}, \quad \mathbf{E} = \begin{bmatrix} 0 \\ -\lambda_m/L_q \\ 0 \\ 0 \end{bmatrix}$$

Making the transfer function, by using laplace operator $s = \frac{d}{dt}$, the measuring matrix $\mathbf{C} = \begin{bmatrix} 1 & 0 & 0 & 0 \\ 0 & 1 & 0 & 0 \end{bmatrix}$ and

$$\mathbf{x}(s) = \mathbf{C}(s\mathbf{I} - \mathbf{A})^{-1}\mathbf{B}\mathbf{u}(s) + \mathbf{C}(s\mathbf{I} - \mathbf{A})^{-1}\mathbf{E}\mathbf{v}(s)$$

gives

$$\begin{bmatrix} i_d \\ i_q \end{bmatrix} = \begin{bmatrix} \frac{\alpha_c}{s+\alpha_c} & 0 \\ 0 & \frac{\alpha_c}{s+\alpha_c} \end{bmatrix} \begin{bmatrix} i_d^{ref} \\ i_q^{ref} \end{bmatrix} + \begin{bmatrix} 0 \\ \frac{-s\lambda_m}{L_q(s+\alpha_c)^2} \end{bmatrix} \omega_r$$

B.5 Maximum torque per ampere

The optimal torque per ampere scheme was calculated formulating two optimization problems. The maximum torque for a given speed is described by

$$\min \ -1.5 \cdot n_p(\lambda_m i_q + (L_d - L_q)i_d i_q)$$
$$\text{s.t.}$$
$$\sqrt{i_d^2 + i_q^2} = I_{max}$$
$$\sqrt{v_d^2 + v_q^2} \leq V_{base}$$

The stationary voltage equations are used, and the speed is specified in the voltage constraint.

$$v_d = R_s i_d - \omega_r L_q i_q$$

$$v_q = R_s i_q + \omega_r L_d i_d + \omega_r \lambda_m$$

For a given torque lower than the maximum torque, the lowest possible current at which this torque can be delivered is described by:

$$\min \ \sqrt{i_d^2 + i_q^2}$$
$$\text{s.t.}$$
$$1.5 \cdot n_p(\lambda_m i_q + (L_d - L_q)i_d i_q) = T_e$$
$$\sqrt{v_d^2 + v_q^2} \leq V_{base}$$

Matlab uses an active set SQP algorithm, which means that the second order derivatives of the target function is approximated and used in a localized QP problem, with linearized versions of the constrains. Solving these problems was fast and straight forward. More advanced features like ac resistance and saturating inductances may possibly be adopted.

Appendix C

Data

C.1 PMSM motor data

Originally designed for use in a hybrid electric vehicle [28], this motor could be fitted in a small family vehicle. The model is borrowed from [28], but equipped to fit the q axis saturating model used in [32].

Machine PMSM1: three phase, Y connected, 50 kW continuous, 320 V DC link voltage, 2 pole pairs, base speed 1780 rad/sec

$$R_s \approx 7.9 \ m\Omega \qquad \lambda_m \approx 104 \ mWb \quad L_d \approx 0.23 \ mH$$
$$L_{q \ mac} \approx 0.56 \ mH \qquad C_1 \approx 0.100 \qquad C_2 \approx \ -1.010$$

The C_1 and C_2 values where approximated assuming that the q axis inductance begins to saturate around the i_q current needed to produce the torque to deliver 50 kW at (mechanical) base speed. This current is $i_q = (50 \ kW / \frac{1}{2} 1780 \ rad/sec) / (\frac{3}{2} n_p \lambda_m) = 180 \ A$, so the L_q starts to saturate at $i_q = 170 \ A$. Additionally, from [28] it is known that $i_q (160\sqrt{2}) = 0.42 \ mH$.

C.2 EV model data

Vehicle mass	1200 kg
Wheel inertia	0.7 kgm^2
Motor rotor inertia	0.017 kgm^2
Gear ratio	1:14
Connection	Y, floating
Battery voltage	320 V
Thevenin battery resistance	0.233 Ω
Filter capacitor	0.5 F
Filter cap inner resistance	1 mΩ
Switching frequency	5 kHz

C.3 Simulation tools

As a part of this masters thesis, a simulation tool that includes the motor, inverter and battery was sought. The model had to be accurate enough to simulate asymmetrical faults, and quick enough to run a moderate number of simulations.

In order to simulate unsymmetrical faults, the motor must either be modeled in the time-phase domain, or the zero-sequence i_o current must be included in the dq model. Unfortunately in this case, tools like simpowersystems and PLECS generally include a dq rotating reference plane model that assumes symmetrical operation.
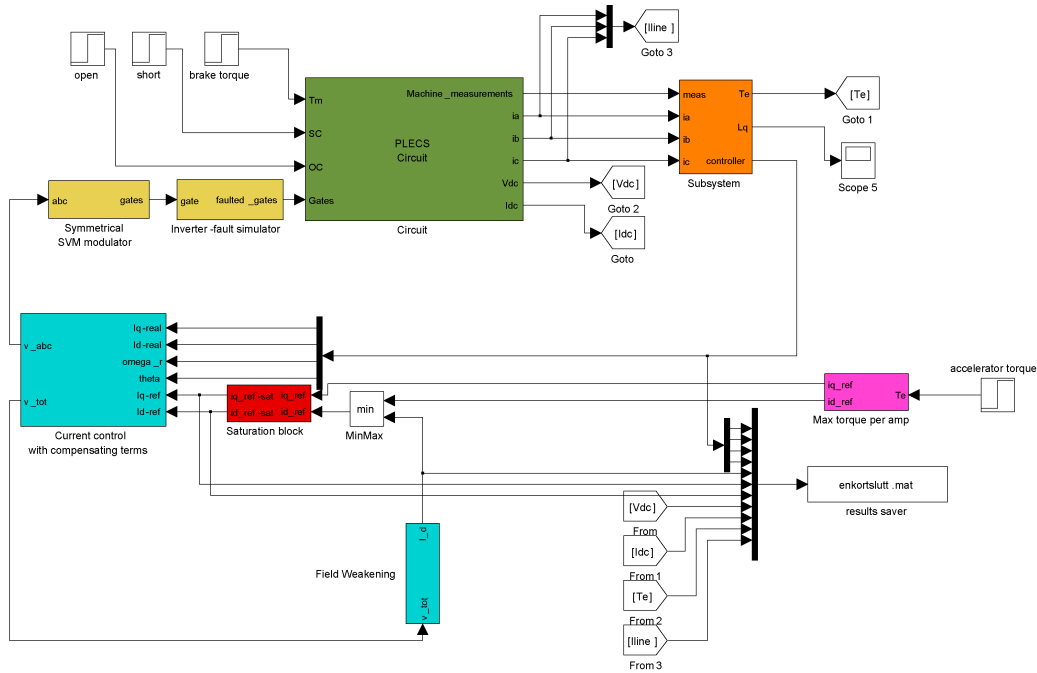

Figure C.1: Simulink EV model. The block "circuit" contains the PLECS inverter and motor model.

C.3.1 PLECS and MATLAB/Simulink

PLECS derives a linear state space model for the circuit at each switching instant. Power electronic switches are basically modeled as a pure open or short circuits, and a switch manager senses switching instants and changes the circuit schematics if switching occurs [Plexim gmbh(2008)].

PLECS contains two motor models for a permanent magnet machine. The PMSM motor block consists of a dq motor model, but it cannot model all the faults well because of underlying assumptions.

PLECS also contains a more general BLDC model, where the back EMF and inductances are specified as functions of the angle in the machine, as Fourier series. This model is capable of simulating asymmetrical faults. This BLDC model was
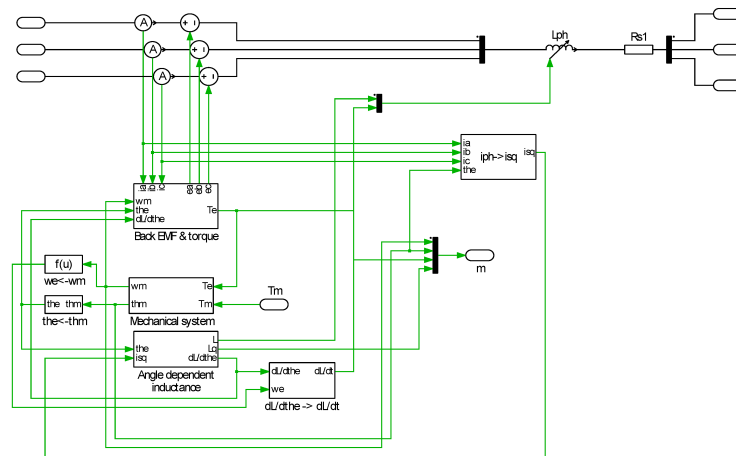
Figure C.2: The inside of the BLDC PLECS block. The library PLECS-block was altered to include saturation of the q axis inductance.

altered to make the neutral point available (for short circuits), and include saturation of the q axis inductance.